iScience

CellPress
OPEN ACCESS

Article

Potent SARS-CoV-2 neutralizing antibodies with therapeutic effects in two animal models

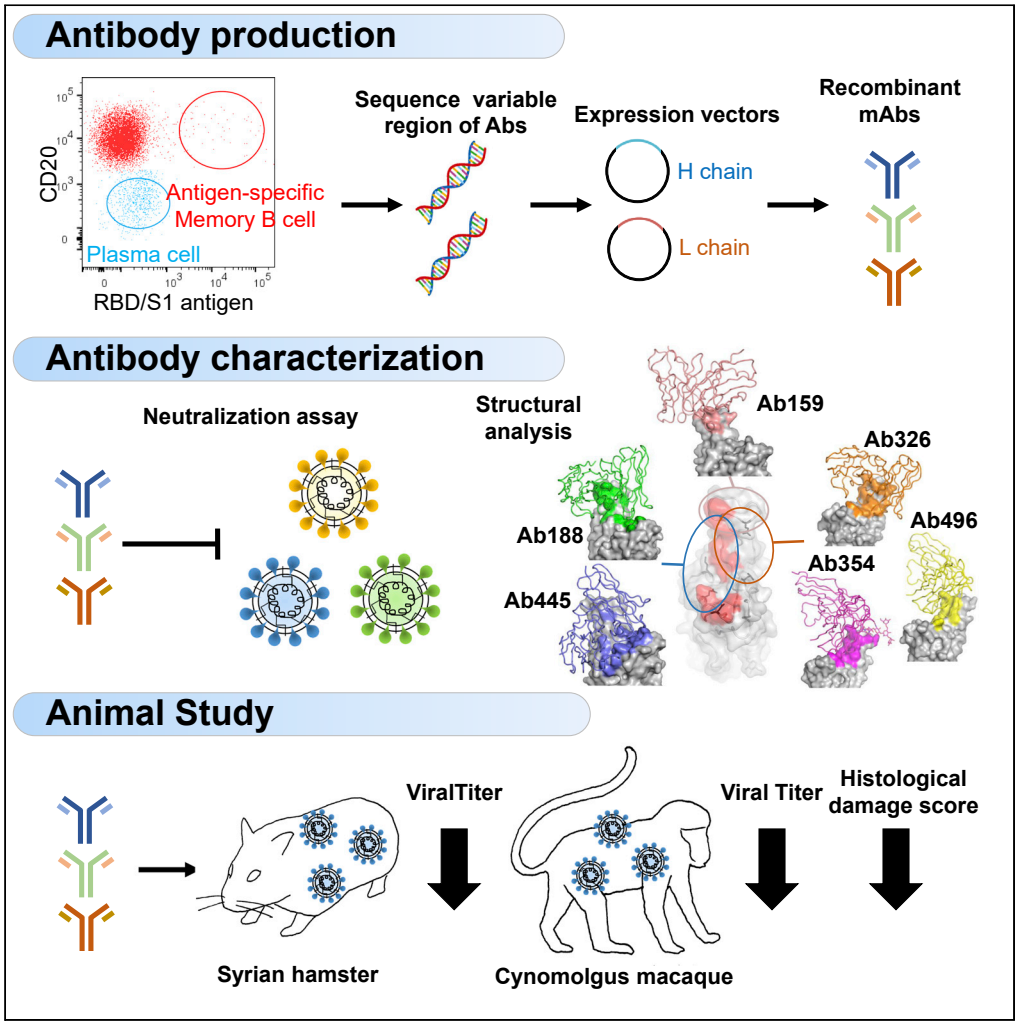

Masaru Takeshita, Hidehiro Fukuyama, Katsuhiko Kamada, ..., Katsuya Suzuki, Koichi Fukunaga, Tsutomu Takeuchi

takeshita@a5.keio.jp

Highlights

Neutralizing antibodies were produced from COVID-19 convalescent peripheral B cells

The structure of the antibodies and their efficacy against variants were demonstrated

N297A modification was introduced to prevent antibody-dependent enhancement

Antibodies showed *in vivo* treatment effects in both hamsters and macaques

Takeshita et al., iScience 25, 105596
December 22, 2022
https://doi.org/10.1016/j.isci.2022.105596

iScience

CellPress
OPEN ACCESS

Article

Potent SARS-CoV-2 neutralizing antibodies with therapeutic effects in two animal models

Masaru Takeshita,[1,17,*] Hidehiro Fukuyama,[2,3,4,5,6] Katsuhiko Kamada,[7,8] Takehisa Matsumoto,[7] Chieko Makino-Okamura,[3] Tomomi Uchikubo-Kamo,[7] Yuri Tomabechi,[7] Kazuharu Hanada,[7] Saya Moriyama,[9] Yoshimasa Takahashi,[9] Hirohito Ishigaki,[10] Misako Nakayama,[10] Cong Thanh Nguyen,[10] Yoshinori Kitagawa,[11] Yasushi Itoh,[10] Masaki Imai,[12,13] Tadashi Maemura,[14] Yuri Furusawa,[12,13] Hiroshi Ueki,[12,13] Kiyoko Iwatsuki-Horimoto,[12] Mutsumi Ito,[12] Seiya Yamayoshi,[12,13] Yoshihiro Kawaoka,[12,13,14] Mikako Shirouzu,[7] Makoto Ishii,[15] Hideyuki Saya,[16] Yasushi Kondo,[1] Yuko Kaneko,[1] Katsuya Suzuki,[1] Koichi Fukunaga,[15] and Tsutomu Takeuchi[1]

SUMMARY

The use of therapeutic neutralizing antibodies against SARS-CoV-2 infection has been highly effective. However, there remain few practical antibodies against viruses that are acquiring mutations. In this study, we created 494 monoclonal antibodies from patients with COVID-19-convalescent, and identified antibodies that exhibited the comparable neutralizing ability to clinically used antibodies in the neutralization assay using pseudovirus and authentic virus including variants of concerns. These antibodies have different profiles against various mutations, which were confirmed by cell-based assay and cryo-electron microscopy. To prevent antibody-dependent enhancement, N297A modification was introduced. Our antibodies showed a reduction of lung viral RNAs by therapeutic administration in a hamster model. In addition, an antibody cocktail consisting of three antibodies was also administered therapeutically to a macaque model, which resulted in reduced viral titers of swabs and lungs and reduced lung tissue damage scores. These results showed that our antibodies have sufficient antiviral activity as therapeutic candidates.

INTRODUCTION

Severe acute respiratory syndrome coronavirus 2 (SARS-CoV-2) continues to spread with the acquisition of various mutations. In Japan, the original Wuhan strain acquired the D614G mutation in the early stages,[1] and was replaced by the more infectious Alpha variant from the end of 2020 to the first half of 2021.[2] Next, it was replaced by the much more infectious Delta variant,[3] and then further replaced by the Omicron variant as of November 2021.[4] Various vaccines have been developed against the Wuhan strains and, fortunately, they have shown efficacy against variants.[5] Although the number of cases has decreased in some countries, probably due to vaccine effectiveness, the global pandemic has not yet been terminated.

The novel coronavirus disease 2019 (COVID-19) is known to progress to a severe state due to excessive immune response and inflammation in the late stages of the disease.[6] Therefore, immunosuppressants, such as steroids, IL-6 inhibitors, and JAK inhibitors, are used in this stage.[7,8] In contrast, in the early stage of infection, there is a period of viral replication, and antiviral therapy is effective during this period. The development of antibody therapies is progressing rapidly, with the Food and Drug Administration (FDA) granting emergency use authorization (EUA) for Regeneron's antibody cocktail (casirivimab and imdevimab), Lilly's antibody (bamlanivimab), the cocktail of bamlanivimab and etesevimab, GSK's sotrovimab, the cocktail of tixagevimab and cilgavimab for prevention, and most recently bebtelovimab monotherapy. These therapies decrease the risk of hospitalization and death by 70%-85%,[9–11] however, the EUA for tixagevimab and cilgavimab and bebtelovimab monotherapy has been revoked because of decreased efficacy against a newly emerged variant of concerns (VOCs). There remain a limited number of treatment options.

[1]Division of Rheumatology, Department of Internal Medicine, Keio University School of Medicine, Tokyo 160-8582, Japan

[2]RIKEN Center for Integrative Medical Sciences, Infectious Diseases Research unit, Kanagawa 230-0045, Japan

[3]RIKEN Center for Integrative Medical Sciences, Laboratory for Lymphocyte Differentiation, Kanagawa 230-0045, Japan

[4]Cell Integrative Science Laboratory, Graduate School of Medical Life Science, Yokohama City University, Kanagawa 230-0045, Japan

[5]INSERM EST, 67037 Strasbourg Cedex 2, France

[6]Near-InfraRed Photo-Immunotherapy Research Institute, Kansai Medical University, Hirakata, Osaka, 573-1010, Japan

[7]RIKEN Center for Biosystems Dynamics Research, Kanagawa 230-0045, Japan

[8]Laboratory for Glycometabolic Biochemistry Laboratory, RIKEN Cluster for Pioneering Research, Saitama 351-0198, Japan

[9]Research Center for Drug and Vaccine Development, National Institute of Infectious Diseases, Tokyo 162-8640, Japan

[10]Department of Pathology, Shiga University of Medical Science, Shiga 520-2192, Japan

[11]Division of Microbiology and Infectious Diseases,

Continued

We have been collecting peripheral blood samples from patients with convalescent since the beginning of the COVID-19 epidemic in Japan in March 2020, from which we started to develop neutralizing antibodies. We have identified several antibodies with neutralizing ability that is equivalent to therapeutic antibodies, and we have demonstrated their efficacy by pseudovirus and authentic virus neutralization assay *in vitro*, and by infection experiments with hamster and macaque models *in vivo*.

RESULTS

Selection of patients with high neutralizing antibody titer

We collected peripheral blood samples from patients with COVID-19 who were discharged from Keio University Hospital. Patient characteristics are shown in Table S1. The neutralization ability of sera was analyzed by cell-based Spike-ACE2 inhibition assay (Figure 1A). From them, we selected 12 patients with high neutralizing titers for antibody production (Figure 1B). Their characteristics are shown in Table S2. From the peripheral blood B cells of these patients, we sorted RBD and S1-binding memory B cells and antigen-nonspecific plasma cells (Figure 1C). The sequences of H-chain and L-chain variable regions were amplified by polymerase chain reaction (PCR), and inserted into expression vectors to produce monoclonal antibodies. A total of 494 antibodies were produced, 408 from antigen-specific memory B cells, and 86 from antigen-nonspecific plasma cells.

Screening of neutralizing antibodies

We screened patient-derived antibodies using two procedures. The first was the Spike-ACE2 inhibition assay described above, in which monoclonal antibodies were used instead of serum. Figure 2A shows the binding ability of the antibodies against Spike-expressing cells and the inhibiting ability of ACE2 to bind to Spike-expressing cells. Spike-binding antibodies were divided into two groups: antibodies that have binding ability without neutralization, as shown by the dotted line, and antibodies that have binding ability correlated with neutralization ability, as shown by the solid line. Figure 2B shows the proportions of antibodies that bind to and neutralize Spike by the source of B cell type. Whereas the small proportion of antibodies produced from antigen-nonspecific plasma cells neutralizes or even bind to Spike-expressing cells, approximately half of the antigen-specific memory B cell-derived antibodies could bind to Spike, 20% bound strongly, 9% had the neutralizing ability, and 3.4% had the high neutralizing ability. These results indicate that neutralizing antibodies can be produced more efficiently from memory B cells than from plasma cells.

In order to perform the screening of these antibodies more robustly, we next examined the neutralizing ability by cell fusion assay, which examines the extent to which antibodies inhibit the fusion of Spike-expressing cells and ACE2-expressing cells. As shown in Figure 2C, the neutralization ability in the cell fusion assay correlated well with that in the Spike-ACE2 inhibition assay.

To confirm that the screened antibodies actually have the ability to neutralize the authentic virus, we performed end-point micro-neutralization assay and determined the minimum concentration of the top 17 antibodies required to neutralize the virus. As shown in Figure 2D, the micro-neutralization titers and ACE2-binding rates were well-correlated, and 11 antibodies were found to be able to completely neutralize authentic virus at a concentration of less than 1 μg/mL.

The effect of point mutation of spike on the neutralizing ability of antibodies

Next, we investigated how the selected antibodies were affected by various mutations in the cell-based Spike-ACE2 inhibition assay using mutated Spike-expressing cells. The ACE2-binding rates of each antibody for mutations within and outside the RBD are shown in Figures 3A and 3B, respectively. Each antibody showed variable neutralizing ability at various sites within the RBD, and these amino acids were considered to be candidates for epitopes. Among them, the E484K mutation affected at least 8 of the top 11 antibodies, and mutation at W406, K417, F456, T478, F486, F490, and Q493 affected 3 to 4 of 11 antibodies. These facts indicate that these positions may be major epitopes of human humoral immunity against the Wuhan-hu-1 strain, consistent with previous reports.[12–14] Because these antibodies were derived from B cells that bind to RBD/S1 and are selected by ACE2 inhibition, it is possible that they were not significantly affected by mutations outside the RBD, including the N-terminal domain (Figure 3B). We also examined the cells expressing Spike, including all variant mutations of SARS-CoV-2 and SARS-CoV-1 (Figure 3C). Although efficacy varies from strain to strain, the Omicron (BA.1) variant has become resistant to almost all antibodies except for Ab188. In addition, the neutralizing ability of any antibodies examined was not observed against SARS-CoV-1.

Department of Pathology, Shiga University of Medical Science, Shiga 520-2192, Japan

[12]Division of Virology, Institute of Medical Science, University of Tokyo, Tokyo 108-8639, Japan

[13]Center for Global Viral Diseases, National Center for Global Health and Medicine, Tokyo 162-8655, Japan

[14]Department of Pathobiological Sciences, School of Veterinary Medicine, University of Wisconsin-Madison, Madison, WI 53706, USA

[15]Division of Pulmonary Medicine, Department of Internal Medicine, Keio University School of Medicine, Tokyo 160-8582, Japan

[16]Division of Gene Regulation, Institute for Advanced Medical Research, Keio University School of Medicine, Tokyo 162-8640, Japan

[17]Lead contact

*Correspondence: takeshita@a5.keio.jp

https://doi.org/10.1016/j.isci.2022.105596

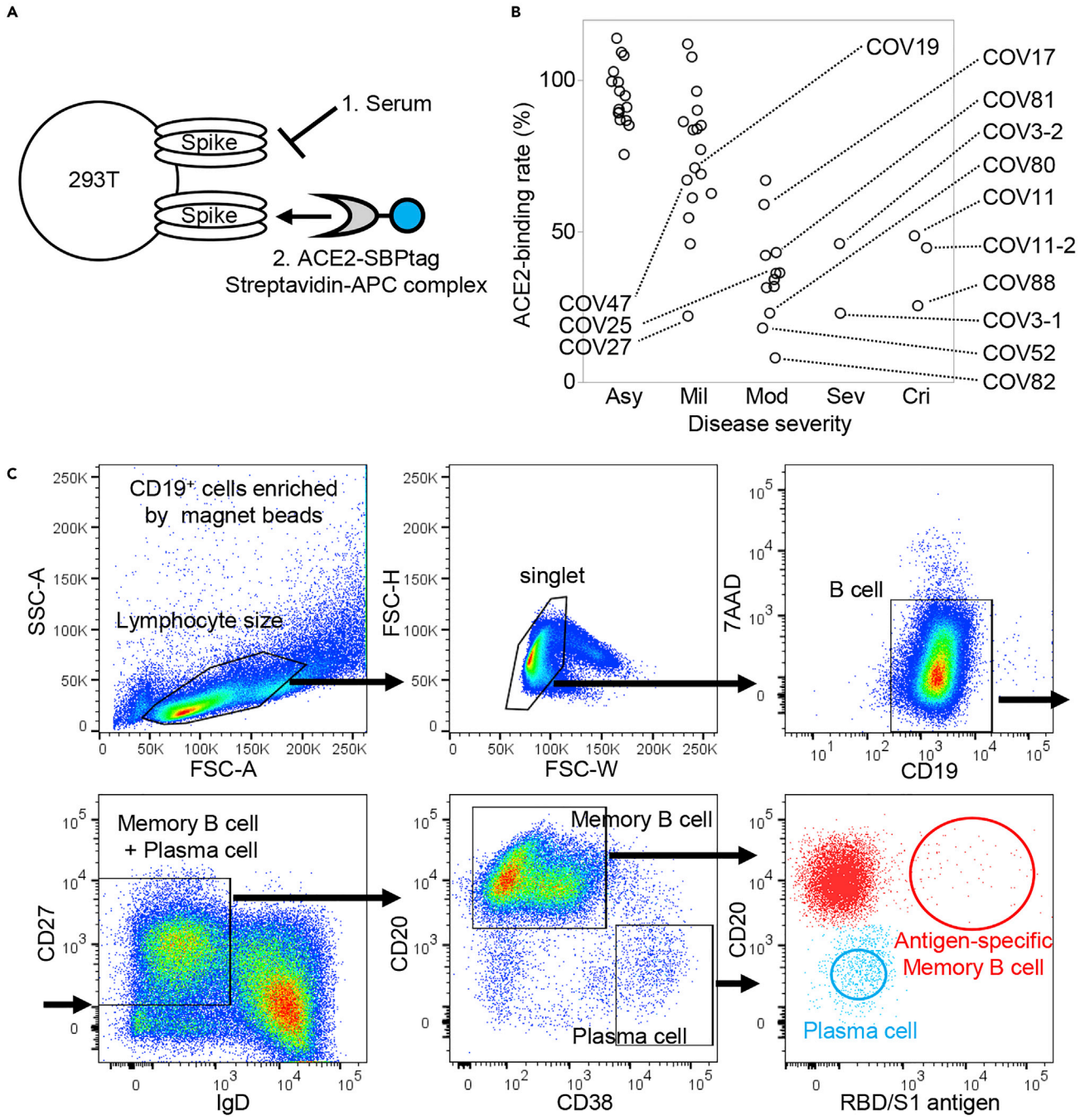

Figure 1. Patient selection and cell sorting

Serum neutralization titers of 47 patients with COVID-19 convalescent were measured by (A) cell-based Spike-ACE2 inhibition assay. The binding quantity of soluble ACE2 to Spike-expressing cells without serum/antibody is defined as 100%, and the binding quantities of soluble ACE2 to Spike-expressing cells after incubation with serum/antibody are calculated as the ACE2-binding rate.

(B) The neutralization ability of patient serum for each severity is shown. Samples used for antibody production are labeled with their ID.

(C) The sorting strategy is shown. $CD19^+$ cells were size gated, and $CD19^+CD27^+IgD^-$ cells were selected. Antigen-specific memory B cells (red) and antigen-nonspecific plasma cells (blue) were single-cell sorted. Asy, asymptomatic; Mil, mild; Mod, moderate; Sev, severe; Cri, critical.

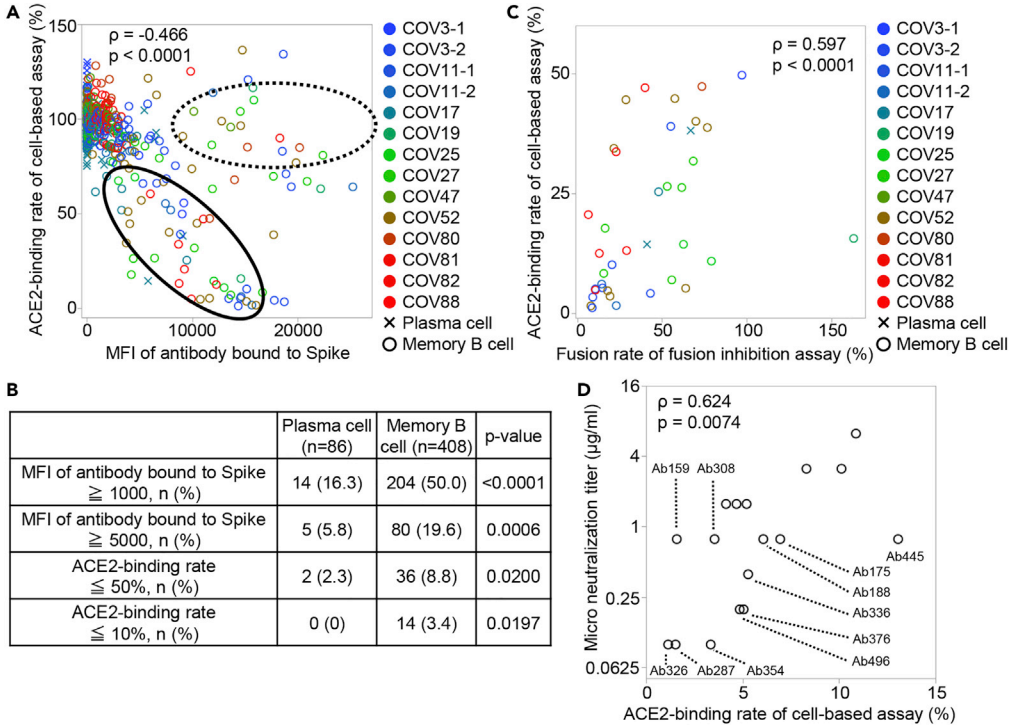

B

	Plasma cell (n=86)	Memory B cell (n=408)	p-value
MFI of antibody bound to Spike ≧ 1000, n (%)	14 (16.3)	204 (50.0)	<0.0001
MFI of antibody bound to Spike ≧ 5000, n (%)	5 (5.8)	80 (19.6)	0.0006
ACE2-binding rate ≦ 50%, n (%)	2 (2.3)	36 (8.8)	0.0200
ACE2-binding rate ≦ 10%, n (%)	0 (0)	14 (3.4)	0.0197

Figure 2. Screening of neutralizing antibodies

(A) The binding ability of the antibodies against Spike-expressing cells, as indicated by mean fluorescence intensity (MFI), and the inhibiting ability of ACE2 to bind to Spike-expressing cells, as indicated by ACE2-binding rate, are shown. Antibodies that have binding ability without neutralization ability are encircled by a dotted line, and antibodies that have a correlation between binding and neutralization ability are encircled by a solid line. Color indicates the individual and shape indicates the cell type from which the antibodies were derived. Spearman's rank correlation coefficient was calculated from all samples.

(B) The percentage of antibodies having high binding ability to Spike and high ability to inhibit ACE2 binding to Spike is shown by the source cell. Chi-squared test.

(C) The neutralization ability of recombinant monoclonal antibody was measured by fusion inhibition assay. The quantity of cell fusion without the antibody is defined as 100%, and the quantity of cell fusion after incubation with antibodies is shown as the fusion rate. The correlation between the ACE2-binding rate and the fusion rate for antibodies with the ACE2-binding rate of 50% or less is shown. Spearman's rank correlation coefficient.

(D) The correlation between the end-point micro-neutralization titer and the ACE2-binding rate is shown. Spearman's rank correlation coefficient.

Considering the possibility of broadening the neutralizing ability of the antibodies by combining antibodies, we also investigated the overlap of the epitopes of these antibodies by Biolayer interferometry. However, all of the top candidate antibodies had overlapping of their epitopes (Figure S1).

Pseudovirus and authentic virus neutralization assay

Before variants of concern (VOCs) appeared, we selected five antibodies and performed a neutralization assay using pseudovirus with Spike protein of the original Wuhan strain and four major variants. The IC_{50} of each antibody was measured compared with the therapeutic antibody imdevimab as a control (Figures 4A and 4B). Ab159, Ab326, Ab354, and Ab496 exhibited similar or better neutralizing ability against Wuhan pseudovirus than the therapeutic antibody. However, Ab159 could not neutralize the Delta variant due to T478K mutation, whereas Ab326, Ab354, and Ab496 could not neutralize the Beta and Gamma variants due to E484K mutation (Figure 3A).

After VOCs appeared, we examined the neutralization abilities of antibodies against the authentic virus of WK-521 and variants, including Alpha, Beta, Gamma, Delta, Kappa, and Omicron BA.1 and BA.2 (Figures 4C and 4D). Similar to the results of pseudovirus, Ab326 and Ab354 were ineffective against the Beta and Gamma variants, and Ab159 was ineffective against the Delta variant. Whereas many antibodies lost neutralizing ability against both Omicron variants, Ab188 retained neutralizing ability. Although the

A

Mutation within the RBD

	Variant	Ab159	Ab175	Ab188	Ab287	Ab308	Ab326	Ab336	Ab354	Ab376	Ab445	Ab496
Wuhan		1.3	2.1	2.6	0.5	4.1	0.4	1.0	0.6	2.3	2.0	0.5
P337R		1.0	5.3	1.7	0.7	12.9	0.3	3.8	0.3	2.6	2.1	0.6
E340A		1.3	2.8	1.7	0.6	14.1	0.3	2.5	0.3	2.7	1.6	0.4
R346K	μ	1.3	4.3	117.9	0.9	11.8	0.5	3.2	1.0	3.5	78.7	1.2
R346S		1.4	2.6	1.3	0.5	10.3	0.3	2.0	0.4	2.7	1.8	0.5
R403K		1.5	4.3	1.3	0.8	12.1	0.3	2.7	0.4	2.5	87.6	0.5
E406W		0.8	1.6	3.2	0.4	9.0	0.4	111.1	0.7	3.0	108.4	10.4
K417N	βο	1.1	19.4	1.3	0.3	2.0	0.3	50.7	0.5	1.8	104.3	0.3
K417E		1.5	29.9	1.3	0.4	1.4	0.4	109.6	0.7	4.9	83.1	0.5
K417T	γ	1.0	7.3	1.2	0.3	2.2	0.3	20.0	0.7	2.1	125.1	0.4
D420N		0.7	9.9	2.8	0.5	19.8	0.2	4.7	0.3	4.5	1.2	0.4
N439K		1.8	3.6	1.6	0.4	15.2	0.3	4.4	0.5	3.1	3.2	0.6
N440K	ο	2.9	4.1	6.0	0.5	11.7	0.4	3.0	0.6	2.7	2.3	0.5
K444Q		1.9	3.2	3.4	0.5	5.2	0.4	0.9	0.6	2.2	1.5	0.4
V445A		1.4	2.0	2.8	0.3	8.6	0.3	1.1	0.5	2.2	1.5	0.3
G446V		1.3	1.7	2.5	0.7	21.8	0.4	1.9	0.6	4.3	4.5	0.6
Y449H		0.3	1.1	0.9	0.2	6.5	0.2	1.0	0.3	1.2	93.4	0.4
N450D		1.6	2.7	3.5	0.4	4.5	0.3	1.1	0.5	1.9	1.4	0.4
L452R	δκ	1.9	2.8	4.8	2.7	79.1	0.6	2.9	0.9	3.8	1.6	0.6
Y453F		2.9	4.2	4.9	0.8	11.0	0.6	8.7	0.7	3.3	1.4	0.7
L455F		1.5	3.4	1.9	0.6	6.2	0.5	88.4	0.6	6.0	33.8	0.4
F456V		19.7	54.3	3.4	0.9	5.1	1.0	3.4	0.9	24.7	5.8	1.1
N460K		1.7	5.4	4.4	0.4	17.8	0.7	2.2	1.4	3.6	2.1	0.9
A475V		2.1	4.2	4.8	0.6	8.2	0.4	2.1	0.6	3.5	3.1	0.6
G476S		6.4	4.4	6.7	0.5	4.6	0.5	1.5	0.6	1.0	2.2	0.5
S477N	ο	68.3	8.5	2.9	0.4	4.4	0.4	1.4	0.5	2.5	2.0	0.4
T478L		60.6	2.1	3.0	0.4	5.3	0.3	1.3	0.6	1.2	2.2	0.6
T478K	δο	81.6	3.1	9.7	0.3	11.4	0.3	3.0	1.2	1.2	2.7	0.6
V483A		4.9	4.3	5.4	1.5	67.7	3.5	2.7	0.4	0.9	2.4	0.9
E484Q	κ	1.1	3.0	4.8	148.7	148.3	28.6	5.8	41.2	3.9	4.7	1.8
E484K	βγηιμ	0.6	1.7	4.6	95.6	96.6	59.9	14.9	99.0	45.3	8.7	103.8
G485D		116.1	3.2	2.0	3.5	8.0	3.0	1.3	2.0	0.9	1.6	118.9
F486V		93.4	3.3	37.0	0.5	13.4	0.5	1.2	0.6	3.0	1.7	110.5
N487T		1.8	2.5	1.9	14.7	98.8	108.4	1.5	0.4	8.0	1.7	4.6
Y489H		0.9	1.5	5.9	0.4	16.5	23.9	107.4	94.0	5.5	0.9	1.5
F490L		1.8	2.5	1.9	14.7	98.8	108.4	1.5	0.4	1.0	1.7	4.6
Q493K	ο	0.9	1.5	5.9	0.4	16.5	23.9	107.4	94.0	5.8	0.9	1.5
S494P		2.2	4.8	6.1	0.4	8.5	1.1	2.1	1.5	1.5	2.3	3.2
Y495H		4.0	3.0	6.4	0.6	11.5	1.5	3.8	2.5	2.0	70.2	2.1
N501Y	αβγομ	2.9	5.1	4.1	0.6	6.9	0.5	5.6	0.6	9.3	92.0	0.7
Y505H	ο	0.4	3.3	1.9	0.3	8.4	0.2	37.1	0.4	0.8	80.9	0.3

B

Mutation outside the RBD

	Variant	Ab159	Ab175	Ab188	Ab287	Ab308	Ab326	Ab336	Ab354	Ab376	Ab445	Ab496
Del69-70	αηο	1.0	3.2	3.6	0.4	3.4	0.3	2.1	0.7	0.8	2.0	0.5
D80A	β	1.8	2.4	2.7	0.4	6.2	0.4	1.7	0.6	0.6	2.1	0.5
D138Y	γ	1.9	2.1	1.5	0.4	2.6	0.4	1.4	0.6	0.7	2.0	0.5
Del144	αη	1.7	2.1	1.7	0.4	5.9	0.3	1.4	0.5	0.5	2.4	0.5
N165Q		4.5	2.8	2.2	0.5	3.4	0.3	2.2	0.8	1.0	2.9	0.6
R190S	γ	3.5	2.7	3.0	0.6	7.8	0.5	1.4	0.9	0.7	2.8	0.6
D215G	β	2.1	4.6	5.1	0.8	13.9	0.7	2.3	1.1	0.9	2.2	0.6
N234Q		6.2	6.9	9.7	1.5	23.0	0.8	8.1	1.5	3.6	5.5	0.7
A570D	α	7.2	1.8	3.2	0.7	5.5	0.6	0.8	0.8	3.9	1.9	0.6
D614G	all	1.3	2.8	4.1	0.5	7.9	0.3	1.6	0.8	0.7	1.4	0.3
H655Y	γο	2.0	3.1	5.6	0.5	7.5	0.4	1.3	0.6	0.7	1.2	0.3
P681H	αιμο	0.9	2.0	2.5	0.5	7.6	0.4	1.5	0.7	0.7	1.6	0.4
R682Q		5.2	2.9	2.7	0.4	15.4	0.3	1.8	0.5	0.5	2.1	0.3
A701V	βι	3.9	2.2	2.3	0.6	7.3	0.5	1.8	0.8	0.7	2.7	0.6
T716I	α	2.1	3.7	4.0	0.5	8.6	0.4	2.2	0.7	0.6	2.4	0.4
S982A	α	4.5	3.2	4.3	0.6	7.6	0.4	2.7	0.8	0.8	1.3	0.4
T1027I	γ	6.6	2.9	5.1	0.9	11.3	0.7	2.2	0.9	1.2	3.3	1.1
D1118H	α	1.9	3.0	3.0	0.4	9.4	0.4	1.6	0.6	0.7	2.1	0.4
V1176F	γ	1.5	2.7	2.4	0.5	4.3	0.4	1.9	0.8	0.9	1.5	0.6

C

	Variant	Ab159	Ab175	Ab188	Ab287	Ab308	Ab326	Ab336	Ab354	Ab376	Ab445	Ab496
Wuhan		1.3	2.1	2.6	0.5	4.1	0.4	1.0	0.6	2.3	2.0	0.5
Alpha		3.0	3.1	3.3	0.3	2.8	0.3	3.3	0.4	2.3	113.7	0.3
Beta		0.6	44.3	2.7	72.3	87.9	53.6	76.5	69.3	85.3	84.5	83.4
Gamma		3.2	66.5	5.5	151.8	137.8	106.6	127.0	127.0	129.3	148.8	117.4
Delta		100.0	4.5	4.7	1.5	109.9	0.7	4.2	0.9	2.4	187.1	0.4
Mu		0.1	0.1	10.4	78.9	92.4	47.3	72.9	100.0	108.2	121.9	96.1
Omicron		73.0	85.4	21.0	73.0	121.8	104.0	78.9	88.8	82.1	100.0	85.4
SARS1		113.3	137.7	125.5	102.7	97.1	107.1	129.5	113	99.1	95.5	86.6

0
10
20
40
100

Figure 3. Effect of point mutation of Spike protein on antibody neutralizing ability

The ACE2-binding rate (%) of recombinant monoclonal antibodies against Spike protein with various point mutations (A) within RBD, (B) outside RBD, and (C) against Spike proteins of VOCs and SARS-CoV-1 were measured by the cell-based Spike-ACE2 inhibition assay. The variant column indicates that the mutation is contained in the VOC and Variants of interest. The numbers indicate the binding quantities of soluble ACE2 to Spike-expressing cells after incubation with antibodies. The color indicates the grade of neutralization ability.

IC_{50} of imdevimab against the Wuhan strain was reported to be 6 to 70 ng/mL,[15–17] our experiments resulted in 320.6 ng/mL, which is higher than previously reported, probably due to the differences in experimental conditions, such as the usage of a sensitive cell-line, VeroE6 cells expressing TMPRSS2.

Cryo-electron microscopy

To gain structural insights into antibodies and the SARS-CoV-2 spike, we performed cryo-electron microscopy (cryo-EM) analysis of complexes with the proline-substituted stable spike (Table S3). In addition to the five selected antibodies, Ab445 was also included in the analysis, as it was assumed to have a different epitope from the others (Figure 3). Single-particle analysis of a series of complexes yielded a better-quality map of a class with the most abundant particles. However, all of the reconstructed densities of the interface between RBD and Fab were poor, probably due to the individual motion of RBD within the spike trimer.

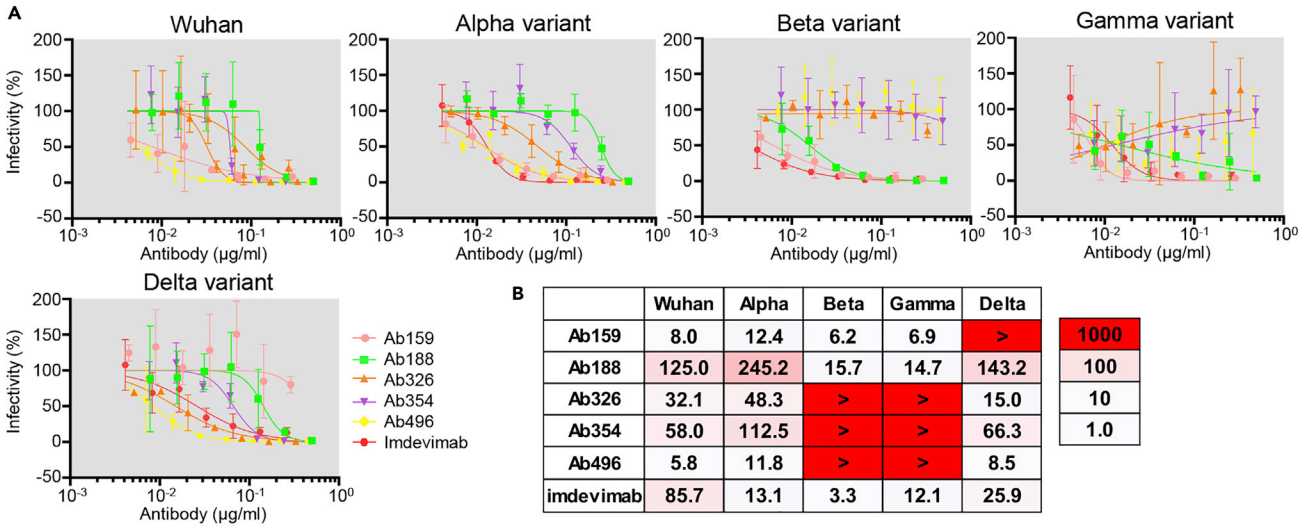

B

	Wuhan	Alpha	Beta	Gamma	Delta
Ab159	8.0	12.4	6.2	6.9	>
Ab188	125.0	245.2	15.7	14.7	143.2
Ab326	32.1	48.3	>	>	15.0
Ab354	58.0	112.5	>	>	66.3
Ab496	5.8	11.8	>	>	8.5
imdevimab	85.7	13.1	3.3	12.1	25.9

1000
100
10
1.0

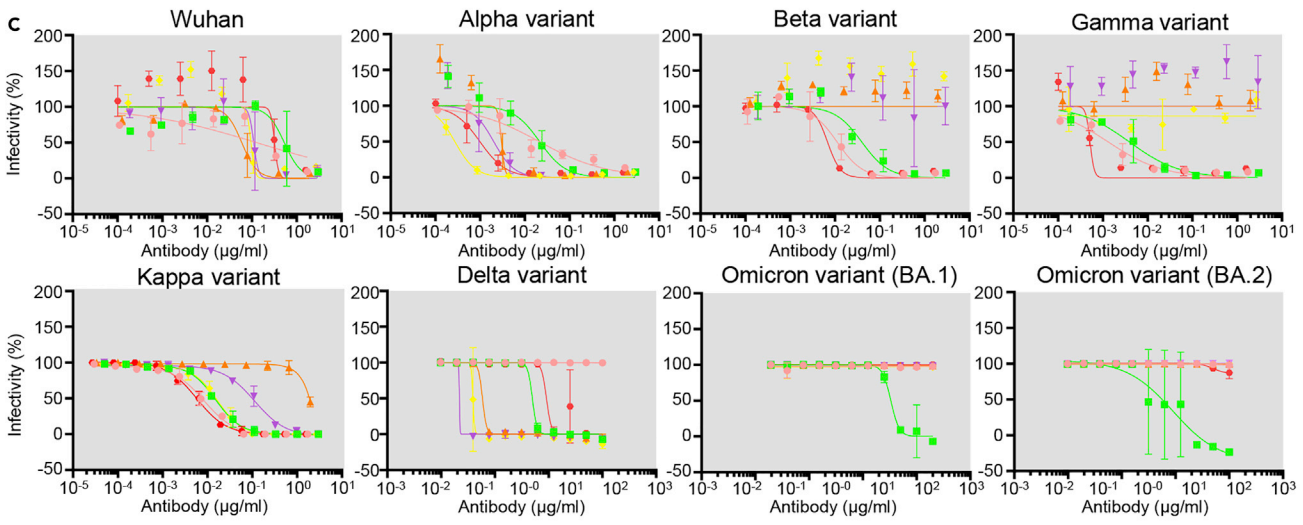

D

	Wuhan	Alpha	Beta	Gamma	Kappa	Delta	BA1	BA2
Ab159	127.9	21.0	11.2	1.3	10.3	>	>	>
Ab188	528.9	21.4	39.8	3.9	18.7	497.4	3320.0	483.5
Ab326	59.5	3.0	>	>	>	58.7	>	>
Ab354	110.0	2.0	>	>	157.6	21.8	>	>
Ab496	95.2	0.3	>	>	23.9	39.0	>	>
imdevimab	320.6	1.0	6.8	0.5	9.1	909.7*	>	>

1000
100
10
1.0

Ab159
Ab188
Ab326
Ab354
Ab496
Imdevimab

Figure 4. Pseudovirus and authentic virus neutralization assay

The IC_{50} (ng/mL) of selected antibodies was measured using pseudovirus that expresses Spike of the Wuhan strain or Alpha, Beta, Gamma, or Delta variants. (A) The neutralization curve and (B) IC_{50} values are shown. The color indicates the neutralizing ability. The data are represented as mean ± SD.

The IC_{50} (ng/mL) of the selected antibodies was examined using authentic virus of the Wuhan strain or Alpha, Beta, Gamma, Delta, Kappa, Omicron (BA.1 and BA.2) variants. (C) Neutralization curve and (D) IC_{50} values are shown. The data are represented as mean ± SD. *Measured separately.

Accordingly, we performed local refinement to improve the density for each Fab-RBD portion, which allows fine modeling of the variable domain of Fab bound to RBD.

In this analysis, the Fab binding location to RBD is roughly classified into three locations (Figure 5A). First, class I type[18] Fabs (Ab188, Ab445) were observed, which access from the same side as the ACE2-binding surface on RBD. Ab326, Ab354, and Ab496 belong to the Class II type antibody that binds from the upper side of RBD. In particular, an *N*-linked glycan was identified at Asn59 of the heavy chain of Ab354 (Figure S2).

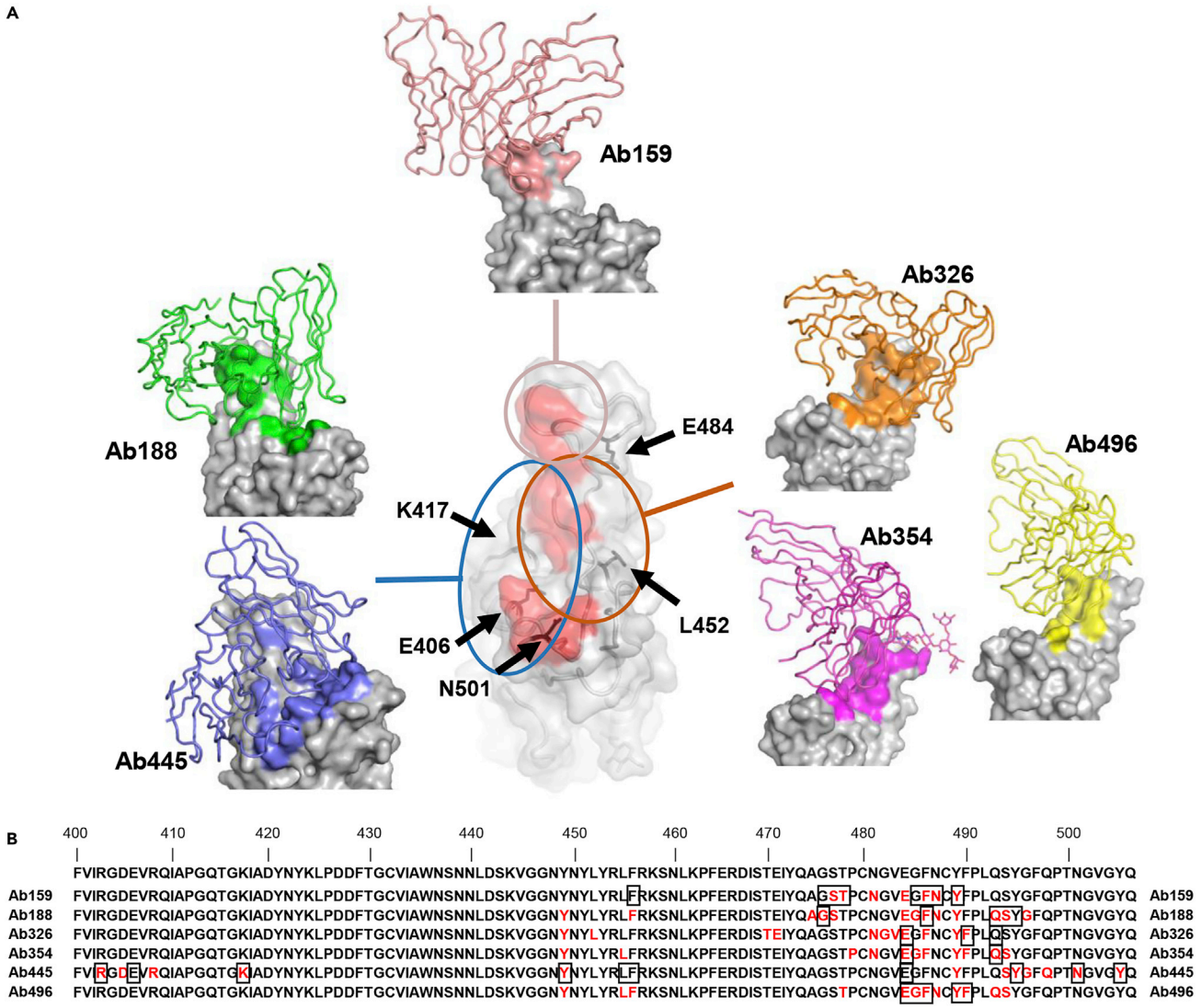

Figure 5. Cryo-EM structure of neutralizing antibodies

(A) The structures of RBD and Ab159, Ab188, Ab326, Ab354, Ab445, and Ab496 are shown. Only the variable domains of antibodies are modeled and drawn as a cartoon tube (individual color) on the RBD surface (gray), and the epitope of each antibody is colored the same as each antibody. The red area in the central RBD is the binding residue of ACE2 (PDB: 7A94),[20] showing the relationship between the binding sites of the antibodies, which are roughly divided into three groups. The positions of key amino acids are indicated by black arrows.

(B) The residues 400-506 of Spike are shown. The epitopes revealed by cryo-EM are colored in red, and the residues affected by the mutation described in Figure 3A are shown in squares.

The fucose moiety of the glycan significantly contributes to binding on the loop region, as previously reported as COVOX-316.[19] A fairly large number of the buried solvent-accessible area per RBD (~1850/ ~1520 Å^2, +sugar/ -sugar) is occupied for this interaction, and each Fab approaches the root of a neighbor RBD.

The third group, Ab159, exclusively binds with the major loop of RBD. Unlike the recently reported antibodies, A23-58.1, B1-182.1,[15] and COVOX-253,[19] Ab159 limitedly recognizes an apex of the loop and mainly interacts only through CDR3 of the heavy chain. The total buried solvent-accessible area is ~1180 Å^2, the smallest area among the analyzed structures (Figure 5A).

We defined the epitope as residues that interact with each other within 4 Å of distance between their respective central atom. Epitopes of each antibody are shown in red in Figure 5B and were localized around residues

Table 1. The affinity of antibodies to RBD

	KD (M)	Kon (/Ms)	Koff (/s)
Ab326	3.46E-11	8.66E+05	3.00E-05
Ab354	5.34E-12	1.58E+06	8.44E-06
Ab496	1.52E-10	1.27E+06	1.93E-04

470-500 of Spike. The residues that affected the neutralizing ability in the Spike-ACE2 inhibition assay described in Figure 3A are marked with squares and are highly consistent with the results of the structural analysis.

Affinity measurement by surface plasmon resonance

To further characterize the selected antibodies, we measured the affinity against RBD protein by SPR. As shown in Table 1, the KDs of the selected antibodies were at sub-nanomolar levels.

Fc-engineering to prevent antibody-dependent enhancement

To avoid the potential risk of interruption of antibody development by ADE, our antibodies used in *in vivo* study had the N297A mutation introduced in the IgG1-Fc region, which reduces binding to the Fc receptor.[21] We checked Fc-mediated antibody uptake before and after the introduction of the N297A mutation using Raji cells. As shown in Figure 6, the antibody without N297A showed Fc-mediated antibody uptake in the concentration range of 1-10 μg/mL whereas the uptake was almost abolished by the introduction of N297A.

In vivo treatment effect in two animal models

We next examined the *in vivo* effects of antibodies in two animal models, a hamster model[22] and a cynomolgus macaque model.[23] Hamsters were infected with the Wuhan strain on day 0 and were intraperitoneally treated with 50 mg/kg BW of an N297A-modified antibody (Ab326, Ab354, or Ab496) or control human IgG1 on day 1. The dose of the antibodies was set at 50 mg/kg. Three days later, the amount of viral RNA in the lung tissue and the neutralizing antibody titer in the serum were measured (Figure 7A). Although antibodies could not be detected in the serum of some hamsters, probably due to technical issues such as administration into the intestinal tract, viral RNA levels in lungs of the hamsters with sera that contained neutralizing antibody titers had reduced (Figure 7B).

Finally, we examined the *in vivo* effects of antibodies in a cynomolgus macaque model. In this study, we used a cocktail of antibodies to cover broader mutations (VOCs had not yet appeared at the time of this study). We mixed equal amounts of Ab326, Ab354, and Ab496, and administrated a total of 20 mg/animal (5-7 mg/kg) the day after infection with a Wuhan strain. Nasal swabs were collected on days 1, 3, 5, and 7, and lung tissue samples were obtained on day 7 (Figure 7C). This model is known to spontaneously recover from COVID-19 in approximately 1 week.[23] Indeed, the live virus in the control IgG1 group became less than detectable range by day 5-7; however, those in all of the animals treated with the mixture of the neutralizing antibodies became undetectable by day 3, earlier than the control group (Figure 7D). We also confirmed that the plasma neutralization titer of the treatment group was higher than that of the control IgG1 group on day 3 (Figure 7E). Finally, the lung tissues were evaluated by viral titer measurement and histological staining. Live virus was partially detected in the lungs of the control group even at day 7 whereas it was undetectable in the treatment group (Figure 7F). Interstitial pneumonia with lymphocytic infiltration and thickened alveolar walls were observed in the control macaques (Figure 7G) whereas such lesions were seen to a lesser extent in the macaques treated with the mixed neutralizing antibodies (Figure 7H). SARS-CoV-2 N protein-positive cell clusters were more frequently detected in the lungs of the control macaques than in the macaques treated with the mixed neutralizing antibodies (Figures 7I and 7J). Histological inflammation scores indicate that treatment with the mixed neutralizing antibodies reduced inflammation in the lungs, consistent with viral titers in the lung tissues (Figure 7K). These results demonstrated the *in vivo* antiviral effects of our antibodies.

DISCUSSION

We have produced many antibodies from the B cells of patients with convalescent of Wuhan or D614G mutant strain, and obtained several neutralizing antibodies with high neutralization ability against variant strains. Initially, antibodies were produced from both antigen-nonspecific plasma cells and

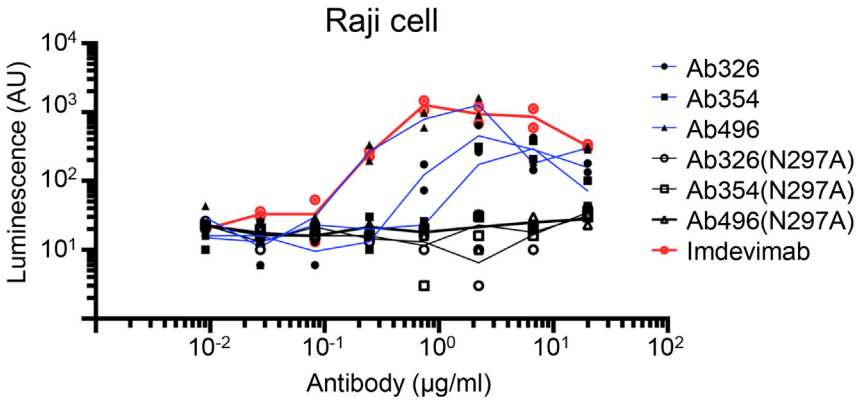

Figure 6. Fc-engineering for the prevention of antibody-dependent enhancement

Pseudovirus (Wuhan strain) was incubated with serially diluted antibody with or without N297A modification, and the mixture was applied to Raji cells. After incubation for 3 days at 37°C, the cells were lysed and subjected to luciferase assay. The lines represent the mean value.

antigen-specific memory B cells, but the latter contained more superior antibodies, suggesting the importance of selecting B cells by antigen. The screening of neutralizing antibodies was performed by the cell-based Spike-ACE2 inhibition assay and cell fusion assay, which correlated with each other, and the results were confirmed by end-point authentic virus neutralization assay. Because antibodies were selected by competition with ACE2, antibody binding to Spike was classified as class 1 or 2, and epitopes on Spike were identified by cell-based mutated Spike-ACE2 inhibition assays and cryo-EM. Results from neutralization assays against Wuhan strain and VOCs using pseudoviruses and authentic viruses confirmed that selected antibodies were equivalent to or superior to imdevimab, which is used as a therapeutic agent. As for the *in vivo* function of these antibodies, efficacy for treatment use was demonstrated in both hamster and macaque models.

Although neutralizing antibodies are used as therapeutic agents and are highly effective, both bamlanivimab and casirivimab reduces susceptibility against E484 mutation,[25] etesevimab reduces susceptibility against K417 mutation,[25] and imdevimab reduces susceptibility against L452R mutation.[15] Most recently, the Omicron variant was demonstrated to reduce the susceptibility of several therapeutic antibodies and antibody cocktails.[26,27] Oral therapeutic agents have also been rapidly developed, however, the fact that a single amino acid mutation in the viral neuraminidase resulted in resistance to neuraminidase inhibitors[28,29] insists on the importance to develop multiple therapeutics targeting various steps of SARS-CoV-2 infection.

One of the characteristics of our antibodies is N297 introduction on IgG1-Fc. This mutation almost eliminates binding to Fc receptors and, indeed, Fc-mediated uptake into Raji cells was eliminated. As for therapeutic antibodies, AZD7442 and etesevimab reduce binding to Fc receptors by YTE and TM modification[30] and LALA modification[31] in the Fc domain, respectively, while bamlanivimab, imdevimab, and casirivimab are unmodified.[31] In contrast, sotrovimab increases binding to FcRn by LS modification.[11] In the absence of Fc receptor binding ability, there is a report that the therapeutic effect is decreased[32] and others that it is not significantly changed,[33] and a consensus has not been established. Although our antibodies are assumed to be less likely to cause ADEs, it is an issue that requires further study to determine which modification is suitable for antiviral therapy.

In conclusion, we produced several potent neutralizing antibodies with high *in vitro* and *in vivo* efficacy. Because the virus is expected to continue to acquire mutations, it is desirable to prepare multiple therapeutic antibodies, and our antibody could be one of the candidates.

Limitations of the study

This study has the following limitations. Because we generated our antibodies from RBD-bound B cells and selected for the inhibition of ACE2 binding to RBD and Spike, there is a bias that non-ACE2 blocking neutralizing antibodies, such as sotrovimab,[34] were not included. The epitopes of our selected antibodies

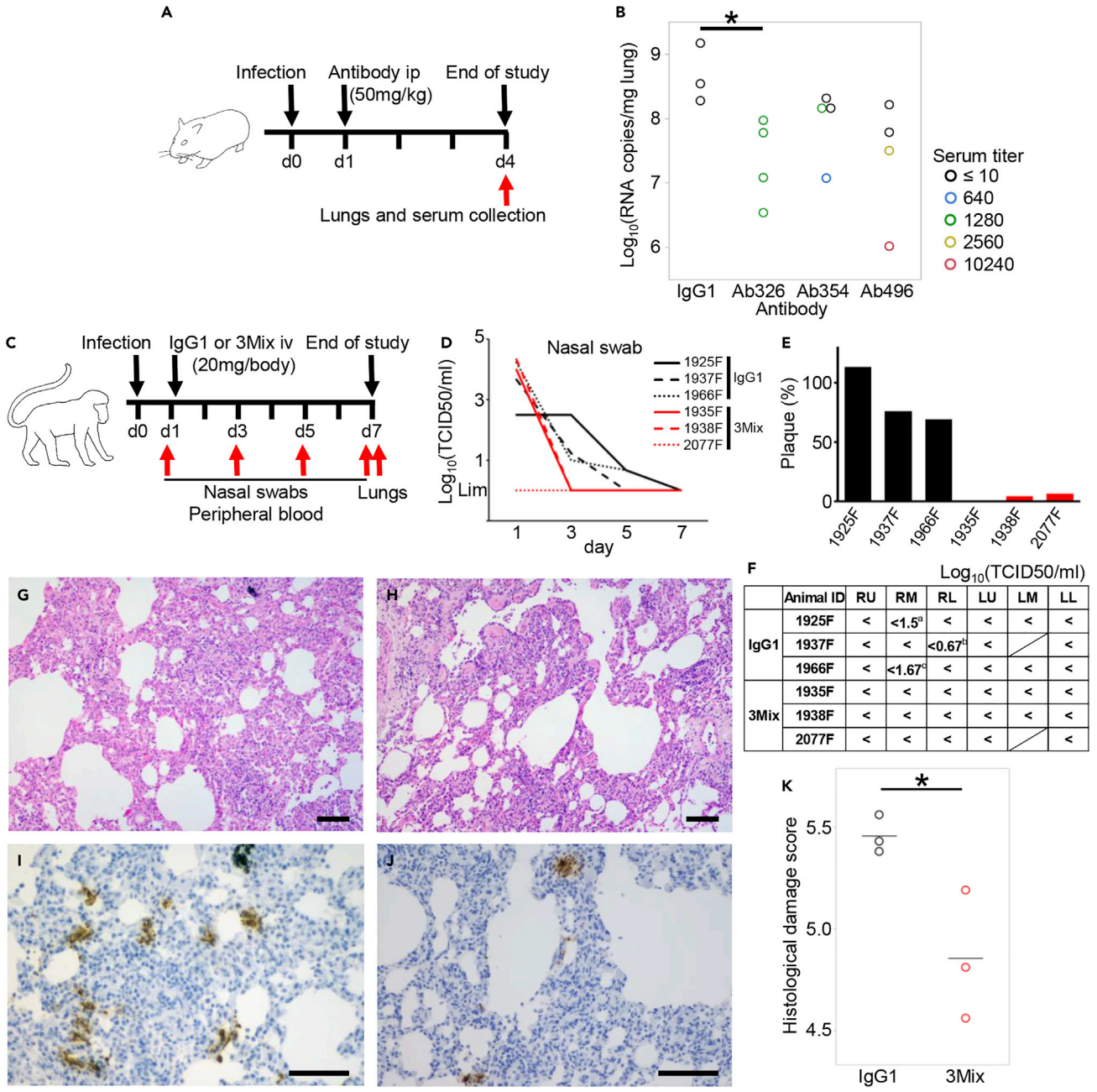

	Animal ID	RU	RM	RL	LU	LM	LL
IgG1	1925F	<	<1.5[a]	<	<	<	<
	1937F	<	<	<0.67[b]	<		<
	1966F	<	<1.67[c]	<	<	<	<
3Mix	1935F	<	<	<	<	<	<
	1938F	<	<	<	<	<	<
	2077F	<	<	<	<		<

Figure 7. Therapeutic efficacy of neutralizing antibodies in two animal models

(A) Overview of the experiment with the Syrian hamster model. Hamsters were inoculated intranasally with 10^3 PFU of NCGM02. On day 1 post-infection, hamsters were injected intraperitoneally with 50 mg/kg BW of neutralizing antibodies or human IgG1 as a control.

(B) On day 4 post-infection, serum and lung samples were collected. Serum-neutralizing titer and viral RNA levels in the lung tissues were measured. Color indicates serum neutralization titer. *$p < 0.05$ by Dunnett's test using all samples.

(C) Overview of the experiment using the cynomolgus macaque model. Six cynomolgus macaques were inoculated with 2×10^7 $TCID_{50}$ SARS-CoV-2 JP/TY/WK-521/2020 into the conjunctiva, nasal cavity, oral cavity, and trachea on day 0. On day 1, 20 mg (5-7 mg/kg) of antibody cocktail 3Mix ($^1/_3$ each of an N297A-modified Ab326, Ab354, and Ab496) or human IgG1 as a control were injected intravenously. Nasal swabs and peripheral blood were collected on days 1, 3, 5, and 7, and lung tissues were collected on day 7.

(D) Viral titers of nasal swabs were measured.

(E) Plasma neutralization titers were measured. The numbers of plaques (%) after antibody administration (day 3) compared to before antibody administration (day 1) are shown.

Figure 7. *Continued*

(F) Viral titers of each lung lobe were measured. "<" indicates under the detection limit. The shaded cells indicate that the lung lobe was not present. [a]CPE-positive wells were 2/4 at no dilution, and 2/4 at 10^1 dilution. [b]CPE-positive wells were 1/4 at no dilution. [c]CPE-positive wells were 1/4 at 10^1 dilution. RU; right upper lobe, RM; right middle lobe, RL; right lower lobe, LU; left upper lobe, LM; left middle lobe, LL; left lower lobe.

(G and H) Representative H&E stained sections and (I and J) immunohistochemical staining of SARS-CoV-2 N protein. (G and I) Lung sections of 1925F were treated with the control antibody. (H and J) Lung sections of 1938F were treated with the mixed SARS-CoV-2 specific neutralizing antibodies. The bars indicate 100 μm.

(K) Histological damage score was evaluated according to the previously published criteria.[24] The bars indicate mean. *$p < 0.05$ by Student's *t* test.

overlaps with one another, and it is difficult to combine them as an antibody cocktail in which antibodies simultaneously bind their respective epitopes on a single molecule of Spike. Meanwhile, there may be advantages in combining antibodies that are weak against different mutations (as in Ab159 and Ab354 in Figure 2A).The unevenly distributed epitopes of the selected antibodies are consistent with previous reports[35,36] that antibodies in the sera of patients infected with Wuhan strains mainly target the area around E484. The number of animals that could be used was limited for both hamsters and macaques, although our antibodies were able to significantly reduce viral titers and tissue damage scores.

STAR★METHODS

Detailed methods are provided in the online version of this paper and include the following:

- KEY RESOURCES TABLE
- RESOURCE AVAILABILITY
  - Lead contact
  - Materials availability
  - Data and code availability
- EXPERIMENTAL MODEL AND SUBJECT DETAILS
  - Ethics statements
  - Animal studies
  - Cells
- METHOD DETAILS
  - Production of vectors and proteins
  - Cell-based Spike-ACE2 inhibition assay
  - Cell sorting
  - Production of antibodies
  - Biolayer interferometry
  - Fusion inhibition assay
  - Endpoint micro neutralization assay
  - Pseudovirus neutralization assay
  - Authentic virus neutralization assay
  - Viral uptake mediated by Fc receptors
  - Production of proteins for cryo-EM
  - Cryo-EM data acquisition
  - Image processing
  - Model building and validation
  - Identification of *N*-glycan composition
  - Surface Plasmon Resonance (SPR) assay
  - Experimental infection of Syrian hamsters
  - Experimental infection of cynomolgus macaques
- QUANTIFICATION AND STATISTICAL ANALYSIS

SUPPLEMENTAL INFORMATION

Supplemental information can be found online at https://doi.org/10.1016/j.isci.2022.105596.

ACKNOWLEDGMENTS

We thank Yukari Kaneda, Mami Yamada, Mayumi Yonemochi, Mariko Ikeda, Mio Inoue, Naoko Kitagawa, and Hideaki Ishida for helping with the experiments, and Ikuo Kawamoto, Takahiro Nakagawa, Hideaki Tsuchiya, and Iori Itagaki for animal care. We also thank Dr. Takehiro Suzuki (Biomolecular Characterization

Unit, RIKEN CSRS) for glycosylation analysis by mass spectrometry. The cryo-EM experiments were performed at the cryo-EM facility of the RIKEN Center for Biosystems Dynamics Research Yokohama. This study was supported by the Collaborative Research Resources, Keio University School of Medicine, and was funded by a research grant for COVID-19 in Keio University School of Medicine (Donner Research Project Grant); by AMED under Grant Numbers JP20fk0108283, JP21ym0126022, and JP21fk0108468; by the RIKEN President's discretionary funds; and by the Mitsubishi Foundation.

AUTHOR CONTRIBUTIONS

M.T., H.S., Y.Kaneko, K.S. T.T. co-ordinated all of the research activities. M.T. wrote the initial draft of the article. Y.T., M.S., K.K., and Y.I. contributed to the editing of the article. H.S., M.Ishii, Y.Kondo, and K.F. contributed to the sample collection. M.T. performed cell-based Spike-ACE2 inhibition assay, cell sorting and antibody production, and biolayer interferometry. S.M. and Y.Takahashi performed the authentic virus neutralization assay. H.F. performed the fusion inhibition assay, pseudovirus/authentic virus neutralization assay, and viral uptake measurement by Fc receptors. C.M–O performed pseudovirus neutralization assay. M.S., K.K., and T.U. performed cryo-EM analysis. T.Matsumoto, Y.Tomabechi., K.H. prepared recombinant antibodies and spike trimer protein. M.Imai, T.Maemura, Y.F., H.U., K.I-H., M.I., S.Y., Y.Kawaoka, and M.T. performed the studies in Syrian hamsters. M.T., H.I., M.N., C.T.N., Y.Kitagawa, and Y.I. performed the infection study of cynomolgus macaques.

DECLARATION OF INTERESTS

M.T., K.S., H.S., T.T., Y.T., S.M., H.F., M.S., T.M., K.K., Y.I., H.I., M.N., Y.Kitagawa, and Y.Kawaoka declared that they are co-inventors on a patent application on neutralizing antibodies described in this article (PCT/JP2021/35159). The remaining authors have no declarations of interest.

Received: May 31, 2022
Revised: October 7, 2022
Accepted: November 10, 2022
Published: December 22, 2022

REFERENCES

1. Korber, B., Fischer, W.M., Gnanakaran, S., Yoon, H., Theiler, J., Abfalterer, W., Hengartner, N., Giorgi, E.E., Bhattacharya, T., Foley, B., et al. (2020). Tracking changes in SARS-CoV-2 spike: evidence that D614G increases Infectivity of the COVID-19 virus. Cell *182*, 812–827.e19. https://doi.org/10.1016/j.cell.2020.06.043.

2. Volz, E., Mishra, S., Chand, M., Barrett, J.C., Johnson, R., Geidelberg, L., Hinsley, W.R., Laydon, D.J., Dabrera, G., O'Toole, A., et al. (2021). Assessing transmissibility of SARS-CoV-2 lineage B.1.1.7 in England. Nature *593*, 266–269. https://doi.org/10.1038/s41586-021-03470-x.

3. Earnest, R., Uddin, R., Matluk, N., Renzette, N., Siddle, K.J., Loreth, C., Adams, G., Tomkins-Tinch, C.H., Petrone, M.E., Rothman, J.E., et al. (2021). Comparative transmissibility of SARS-CoV-2 variants Delta and Alpha in New England, USA. Preprint at medRxiv. https://doi.org/10.1101/2021.10.06.21264641.

4. Shah, M., and Woo, H.G. (2022). Omicron: a heavily mutated SARS-CoV-2 variant exhibits stronger binding to ACE2 and potently escapes approved COVID-19 therapeutic antibodies. Front. Immunol. *12*. https://doi.org/10.3389/fimmu.2021.830527.

5. Thomas, S.J., Moreira, E.D., Jr., Kitchin, N., Absalon, J., Gurtman, A., Lockhart, S., Perez, J.L., Pérez Marc, G., Polack, F.P., Zerbini, C., et al. (2021). Safety and efficacy of the BNT162b2 mRNA Covid-19 vaccine through 6 months. N. Engl. J. Med. *385*, 1761–1773. https://doi.org/10.1056/NEJMoa2110345.

6. Siddiqi, H.K., and Mehra, M.R. (2020). COVID-19 illness in native and immunosuppressed states: a clinical-therapeutic staging proposal. J. Heart Lung Transplant. *39*, 405–407. https://doi.org/10.1016/j.healun.2020.03.012.

7. Yokota, S., Miyamae, T., Kuroiwa, Y., and Nishioka, K. (2021). Novel coronavirus disease 2019 (COVID-19) and cytokine storms for more effective treatments from an inflammatory pathophysiology. J. Clin. Med. *10*. https://doi.org/10.3390/jcm10040801.

8. Lowery, S.A., Sariol, A., and Perlman, S. (2021). Innate immune and inflammatory responses to SARS-CoV-2: Implications for COVID-19. Cell Host Microbe *29*, 1052–1062. https://doi.org/10.1016/j.chom.2021.05.004.

9. Dougan, M., Nirula, A., Azizad, M., Mocherla, B., Gottlieb, R.L., Chen, P., Hebert, C., Perry, R., Boscia, J., Heller, B., et al. (2021). Bamlanivimab plus etesevimab in mild or moderate Covid-19. N. Engl. J. Med. *385*, 1382–1392. https://doi.org/10.1056/NEJMoa2102685.

10. Weinreich, D.M., Sivapalasingam, S., Norton, T., Ali, S., Gao, H., Bhore, R., Xiao, J., Hooper, A.T., Hamilton, J.D., Musser, B.J., et al. (2021). REGEN-COV antibody combination and outcomes in outpatients with Covid-19. N. Engl. J. Med. *385*, e81. https://doi.org/10.1056/NEJMoa2108163.

11. Gupta, A., Gonzalez-Rojas, Y., Juarez, E., Crespo Casal, M., Moya, J., Falci, D.R., Sarkis, E., Solis, J., Zheng, H., Scott, N., et al. (2021). Early treatment for Covid-19 with SARS-CoV-2 neutralizing antibody sotrovimab. N. Engl. J. Med. *385*, 1941–1950. https://doi.org/10.1056/NEJMoa2107934.

12. Hoffmann, M., Arora, P., Gross, R., Seidel, A., Hornich, B.F., Hahn, A.S., Kruger, N., Graichen, L., Hofmann-Winkler, H., Kempf, A., et al. (2021). SARS-CoV-2 variants B.1.351 and P.1 escape from neutralizing antibodies. Cell *184*, 2384–2393.e12. https://doi.org/10.1016/j.cell.2021.03.036.

13. Zhou, D., Dejnirattisai, W., Supasa, P., Liu, C., Mentzer, A.J., Ginn, H.M., Zhao, Y., Duyvesteyn, H.M.E., Tuekprakhon, A., Nutalai, R., et al. (2021). Evidence of escape of SARS-CoV-2 variant B.1.351 from natural and vaccine-induced sera. Cell *184*, 2348–2361.e6. https://doi.org/10.1016/j.cell.2021.02.037.

14. Wang, P., Casner, R.G., Nair, M.S., Wang, M., Yu, J., Cerutti, G., Liu, L., Kwong, P.D., Huang,

Y., Shapiro, L., and Ho, D.D. (2021). Increased resistance of SARS-CoV-2 variant P.1 to antibody neutralization. Cell Host Microbe *29*, 747–751.e4. https://doi.org/10.1016/j.chom.2021.04.007.

15. Wang, L., Zhou, T., Zhang, Y., Yang, E.S., Schramm, C.A., Shi, W., Pegu, A., Oloniniyi, O.K., Henry, A.R., Darko, S., et al. (2021). Ultrapotent antibodies against diverse and highly transmissible SARS-CoV-2 variants. Science *373*, eabh1766. https://doi.org/10.1126/science.abh1766.

16. Hansen, J., Baum, A., Pascal, K.E., Russo, V., Giordano, S., Wloga, E., Fulton, B.O., Yan, Y., Koon, K., Patel, K., et al. (2020). Studies in humanized mice and convalescent humans yield a SARS-CoV-2 antibody cocktail. Science *369*, 1010–1014. https://doi.org/10.1126/science.abd0827.

17. Fenwick, C., Turelli, P., Perez, L., Pellaton, C., Esteves-Leuenberger, L., Farina, A., Campos, J., Lana, E., Fiscalini, F., Raclot, C., et al. (2021). A highly potent antibody effective against SARS-CoV-2 variants of concern. Cell Rep. *37*, 109814. https://doi.org/10.1016/j.celrep.2021.109814.

18. Barnes, C.O., Jette, C.A., Abernathy, M.E., Dam, K.A., Esswein, S.R., Gristick, H.B., Malyutin, A.G., Sharaf, N.G., Huey-Tubman, K.E., Lee, Y.E., et al. (2020). SARS-CoV-2 neutralizing antibody structures inform therapeutic strategies. Nature *588*, 682–687. https://doi.org/10.1038/s41586-020-2852-1.

19. Dejnirattisai, W., Zhou, D., Ginn, H.M., Duyvesteyn, H.M.E., Supasa, P., Case, J.B., Zhao, Y., Walter, T.S., Mentzer, A.J., Liu, C., et al. (2021). The antigenic anatomy of SARS-CoV-2 receptor binding domain. Cell *184*, 2183–2200.e22. https://doi.org/10.1016/j.cell.2021.02.032.

20. Benton, D.J., Wrobel, A.G., Xu, P., Roustan, C., Martin, S.R., Rosenthal, P.B., Skehel, J.J., and Gamblin, S.J. (2020). Receptor binding and priming of the spike protein of SARS-CoV-2 for membrane fusion. Nature *588*, 327–330. https://doi.org/10.1038/s41586-020-2772-0.

21. Chao, D.T., Ma, X., Li, O., Park, H., and Law, D. (2009). Functional characterization of N297A, a murine surrogate for low-Fc binding anti-human CD3 antibodies. Immunol. Invest. *38*, 76–92. https://doi.org/10.1080/08820130802608238.

22. Imai, M., Iwatsuki-Horimoto, K., Hatta, M., Loeber, S., Halfmann, P.J., Nakajima, N., Watanabe, T., Ujie, M., Takahashi, K., Ito, M., et al. (2020). Syrian hamsters as a small animal model for SARS-CoV-2 infection and countermeasure development. Proc. Natl. Acad. Sci. USA *117*, 16587–16595. https://doi.org/10.1073/pnas.2009799117.

23. Ishigaki, H., Nakayama, M., Kitagawa, Y., Nguyen, C.T., Hayashi, K., Shiohara, M., Gotoh, B., and Itoh, Y. (2021). Neutralizing antibody-dependent and -independent immune responses against SARS-CoV-2 in cynomolgus macaques. Virology *554*, 97–105. https://doi.org/10.1016/j.virol.2020.12.013.

24. Ogiwara, H., Yasui, F., Munekata, K., Takagi-Kamiya, A., Munakata, T., Nomura, N., Shibasaki, F., Kuwahara, K., Sakaguchi, N., Sakoda, Y., et al. (2014). Histopathological evaluation of the diversity of cells susceptible to H5N1 virulent avian influenza virus. Am. J. Pathol. *184*, 171–183. https://doi.org/10.1016/j.ajpath.2013.10.004.

25. Starr, T.N., Greaney, A.J., Dingens, A.S., and Bloom, J.D. (2021). Complete map of SARS-CoV-2 RBD mutations that escape the monoclonal antibody LY-CoV555 and its cocktail with LY-CoV016. Cell Rep. Med. *2*, 100255. https://doi.org/10.1016/j.xcrm.2021.100255.

26. Cameroni, E., Bowen, J.E., Rosen, L.E., Saliba, C., Zepeda, S.K., Culap, K., Pinto, D., VanBlargan, L.A., De Marco, A., di Iulio, J., et al. (2021). Broadly neutralizing antibodies overcome SARS-CoV-2 Omicron antigenic shift. Nature *602*, 664–670. https://doi.org/10.1038/s41586-021-04386-2.

27. Planas, D., Saunders, N., Maes, P., Guivel-Benhassine, F., Planchais, C., Buchrieser, J., Bolland, W.H., Porrot, F., Staropoli, I., Lemoine, F., et al. (2021). Considerable escape of SARS-CoV-2 Omicron to antibody neutralization. Nature *602*, 671–675. https://doi.org/10.1038/s41586-021-04389-z.

28. Lee, N., and Hurt, A.C. (2018). Neuraminidase inhibitor resistance in influenza: a clinical perspective. Curr. Opin. Infect. Dis. *31*, 520–526. https://doi.org/10.1097/QCO.0000000000000498.

29. Dapat, C., Kondo, H., Dapat, I.C., Baranovich, T., Suzuki, Y., Shobugawa, Y., Saito, K., Saito, R., and Suzuki, H. (2013). Neuraminidase inhibitor susceptibility profile of pandemic and seasonal influenza viruses during the 2009-2010 and 2010-2011 influenza seasons in Japan. Antivir. Res. *99*, 261–269. https://doi.org/10.1016/j.antiviral.2013.06.003.

30. Loo, Y.-M., McTamney, P.M., Arends, R.H., Gasser, R.A., Abram, M.E., Aksyuk, A., Diallo, S., Flores, D.J., Kelly, E.J., Ren, K., et al. (2021). AZD7442 demonstrates prophylactic and therapeutic efficacy in non-human primates and extended half-life in humans. Preprint at medRxiv. https://doi.org/10.1101/2021.08.30.21262666.

31. Taylor, P.C., Adams, A.C., Hufford, M.M., de la Torre, I., Winthrop, K., and Gottlieb, R.L. (2021). Neutralizing monoclonal antibodies for treatment of COVID-19. Nat. Rev. Immunol. *21*, 382–393. https://doi.org/10.1038/s41577-021-00542-x.

32. Chan, C.E.Z., Seah, S.G.K., Chye, H., Massey, S., Torres, M., Lim, A.P.C., Wong, S.K.K., Neo, J.J.Y., Wong, P.S., Lim, J.H., et al. (2021). The Fc-mediated effector functions of a potent SARS-CoV-2 neutralizing antibody, SC31, isolated from an early convalescent COVID-19 patient, are essential for the optimal therapeutic efficacy of the antibody. PLoS One *16*, e0253487. https://doi.org/10.1371/journal.pone.0253487.

33. Noy-Porat, T., Edri, A., Alcalay, R., Makdasi, E., Gur, D., Aftalion, M., Evgy, Y., Beth-Din, A., Levy, Y., Epstein, E., et al. (2021). Fc-Independent Protection from SARS-CoV-2 infection by recombinant human monoclonal antibodies. Antibodies *10*, 45. https://doi.org/10.3390/antib10040045.

34. Pinto, D., Park, Y.J., Beltramello, M., Walls, A.C., Tortorici, M.A., Bianchi, S., Jaconi, S., Culap, K., Zatta, F., De Marco, A., et al. (2020). Cross-neutralization of SARS-CoV-2 by a human monoclonal SARS-CoV antibody. Nature *583*, 290–295. https://doi.org/10.1038/s41586-020-2349-y.

35. Greaney, A.J., Loes, A.N., Crawford, K.H.D., Starr, T.N., Malone, K.D., Chu, H.Y., and Bloom, J.D. (2021). Comprehensive mapping of mutations in the SARS-CoV-2 receptor-binding domain that affect recognition by polyclonal human plasma antibodies. Cell Host Microbe *29*, 463–476.e6. https://doi.org/10.1016/j.chom.2021.02.003.

36. Piccoli, L., Park, Y.J., Tortorici, M.A., Czudnochowski, N., Walls, A.C., Beltramello, M., Silacci-Fregni, C., Pinto, D., Rosen, L.E., Bowen, J.E., et al. (2020). Mapping neutralizing and immunodominant sites on the SARS-CoV-2 spike receptor-binding domain by structure-guided high-resolution serology. Cell *183*, 1024–1042.e21. https://doi.org/10.1016/j.cell.2020.09.037.

37. Takeshita, M., Nishina, N., Moriyama, S., Takahashi, Y., Uwamino, Y., Nagata, M., Aoki, W., Masaki, K., Ishii, M., Saya, H., et al. (2021). Incomplete humoral response including neutralizing antibodies in asymptomatic to mild COVID-19 patients in Japan. Virology *555*, 35–43. https://doi.org/10.1016/j.virol.2020.12.020.

38. Takeshita, M., Suzuki, K., Kondo, Y., Morita, R., Okuzono, Y., Koga, K., Kassai, Y., Gamo, K., Takiguchi, M., Kurisu, R., et al. (2019). Multi-dimensional analysis identified rheumatoid arthritis-driving pathway in human T cell. Ann. Rheum. Dis. *78*, 1346–1356. https://doi.org/10.1136/annrheumdis-2018-214885.

39. Picelli, S., Faridani, O.R., Bjorklund, A.K., Winberg, G., Sagasser, S., and Sandberg, R. (2014). Full-length RNA-seq from single cells using Smart-seq2. Nat. Protoc. *9*, 171–181. https://doi.org/10.1038/nprot.2014.006.

40. Takeshita, M., Suzuki, K., Nakazawa, M., Kamata, H., Ishii, M., Oyamada, Y., Oshima, H., and Takeuchi, T. (2021). Antigen-driven autoantibody production in lungs of interstitial lung disease with autoimmune disease. J. Autoimmun. *121*, 102661. https://doi.org/10.1016/j.jaut.2021.102661.

41. Takeshita, M., Suzuki, K., Kaneda, Y., Yamane, H., Ikeura, K., Sato, H., Kato, S., Tsunoda, K., Arase, H., and Takeuchi, T. (2020). Antigen-driven selection of antibodies against SSA, SSB and the centromere 'complex', including a novel antigen, MIS12 complex, in human salivary glands. Ann. Rheum. Dis. *79*, 150–158. https://doi.org/10.1136/annrheumdis-2019-215862.

42. Yamamoto, M., Kiso, M., Sakai-Tagawa, Y., Iwatsuki-Horimoto, K., Imai, M., Takeda, M., Kinoshita, N., Ohmagari, N., Gohda, J., Semba, K., et al. (2020). The Anticoagulant Nafamostat potently inhibits SARS-CoV-2 S protein-mediated fusion in a cell fusion assay

system and viral infection in vitro in a cell-type-dependent manner. Viruses *12*, 629. https://doi.org/10.3390/v12060629.

43. Matsuyama, S., Nao, N., Shirato, K., Kawase, M., Saito, S., Takayama, I., Nagata, N., Sekizuka, T., Katoh, H., Kato, F., et al. (2020). Enhanced isolation of SARS-CoV-2 by TMPRSS2-expressing cells. Proc. Natl. Acad. Sci. USA *117*, 7001–7003. https://doi.org/10.1073/pnas.2002589117.

44. Moriyama, S., Adachi, Y., Sato, T., Tonouchi, K., Sun, L., Fukushi, S., Yamada, S., Kinoshita, H., Nojima, K., Kanno, T., et al. (2021). Temporal maturation of neutralizing antibodies in COVID-19 convalescent individuals improves potency and breadth to circulating SARS-CoV-2 variants. Immunity *54*, 1841–1852.e4. https://doi.org/10.1016/j.immuni.2021.06.015.

45. Hsieh, C.L., Goldsmith, J.A., Schaub, J.M., DiVenere, A.M., Kuo, H.C., Javanmardi, K., Le, K.C., Wrapp, D., Lee, A.G., Liu, Y., et al. (2020). Structure-based design of prefusion-stabilized SARS-CoV-2 spikes. Science *369*, 1501–1505. https://doi.org/10.1126/science.abd0826.

46. Arimori, T., Kitago, Y., Umitsu, M., Fujii, Y., Asaki, R., Tamura-Kawakami, K., and Takagi, J. (2017). Fv-clasp: an artificially designed small antibody fragment with improved production compatibility, stability, and crystallizability. Structure *25*, 1611–1622.e4. https://doi.org/10.1016/j.str.2017.08.011.

47. Katsura, K., Matsuda, T., Tomabechi, Y., Yonemochi, M., Hanada, K., Ohsawa, N., Sakamoto, K., Takemoto, C., and Shirouzu, M. (2017). A reproducible and scalable procedure for preparing bacterial extracts for cell-free protein synthesis. J. Biochem. *162*, 357–369. https://doi.org/10.1093/jb/mvx039.

48. Matsuda, T., Ito, T., Takemoto, C., Katsura, K., Ikeda, M., Wakiyama, M., Kukimoto-Niino, M., Yokoyama, S., Kurosawa, Y., and Shirouzu, M. (2018). Cell-free synthesis of functional antibody fragments to provide a structural basis for antibody-antigen interaction. PLoS One *13*, e0193158. https://doi.org/10.1371/journal.pone.0193158.

49. Zivanov, J., Nakane, T., Forsberg, B.O., Kimanius, D., Hagen, W.J., Lindahl, E., and Scheres, S.H. (2018). New tools for automated high-resolution cryo-EM structure determination in RELION-3. Elife *7*, e42166. https://doi.org/10.7554/eLife.42166.

50. Zheng, S.Q., Palovcak, E., Armache, J.P., Verba, K.A., Cheng, Y., and Agard, D.A. (2017). MotionCor2: anisotropic correction of beam-induced motion for improved cryo-electron microscopy. Nat. Methods *14*, 331–332. https://doi.org/10.1038/nmeth.4193.

51. Rohou, A., and Grigorieff, N. (2015). CTFFIND4: fast and accurate defocus estimation from electron micrographs. J. Struct. Biol. *192*, 216–221. https://doi.org/10.1016/j.jsb.2015.08.008.

52. Wagner, T., Merino, F., Stabrin, M., Moriya, T., Antoni, C., Apelbaum, A., Hagel, P., Sitsel, O., Raisch, T., Prumbaum, D., et al. (2019). SPHIRE-crYOLO is a fast and accurate fully automated particle picker for cryo-EM. Commun. Biol. *2*, 218. https://doi.org/10.1038/s42003-019-0437-z.

53. Liebschner, D., Afonine, P.V., Baker, M.L., Bunkóczi, G., Chen, V.B., Croll, T.I., Hintze, B., Hung, L.W., Jain, S., McCoy, A.J., et al. (2019). Macromolecular structure determination using X-rays, neutrons and electrons: recent developments in Phenix. Acta Crystallogr. D Struct. Biol. *75*, 861–877. https://doi.org/10.1107/s2059798319011471.

54. Emsley, P., Lohkamp, B., Scott, W.G., and Cowtan, K. (2010). Features and development of coot. Acta Crystallogr. D Struct. Biol. *66*, 486–501. https://doi.org/10.1107/s0907444910007493.

55. Waterhouse, A., Bertoni, M., Bienert, S., Studer, G., Tauriello, G., Gumienny, R., Heer, F.T., de Beer, T.A.P., Rempfer, C., Bordoli, L., et al. (2018). SWISS-MODEL: homology modelling of protein structures and complexes. Nucleic Acids Res. *46*. W296–w303. https://doi.org/10.1093/nar/gky427.

56. Williams, C.J., Headd, J.J., Moriarty, N.W., Prisant, M.G., Videau, L.L., Deis, L.N., Verma, V., Keedy, D.A., Hintze, B.J., Chen, V.B., et al. (2018). MolProbity: more and better reference data for improved all-atom structure validation. Protein Sci. *27*, 293–315. https://doi.org/10.1002/pro.3330.

57. Goddard, T.D., Huang, C.C., Meng, E.C., Pettersen, E.F., Couch, G.S., Morris, J.H., and Ferrin, T.E. (2018). UCSF ChimeraX: meeting modern challenges in visualization and analysis. Protein Sci. *27*, 14–25. https://doi.org/10.1002/pro.3235.

58. Davydova, E., Shimazu, T., Schuhmacher, M.K., Jakobsson, M.E., Willemen, H., Liu, T., Moen, A., Ho, A.Y.Y., Małecki, J., Schroer, L., et al. (2021). The methyltransferase METTL9 mediates pervasive 1-methylhistidine modification in mammalian proteomes. Nat. Commun. *12*, 891. https://doi.org/10.1038/s41467-020-20670-7.

59. Mariethoz, J., Alocci, D., Gastaldello, A., Horlacher, O., Gasteiger, E., Rojas-Macias, M., Karlsson, N.G., Packer, N.H., and Lisacek, F. (2018). Glycomics@ExPASy: bridging the gap. Mol. Cell. Proteomics *17*, 2164–2176. https://doi.org/10.1074/mcp.RA118.000799.

STAR★METHODS

KEY RESOURCES TABLE

REAGENT or RESOURCE	SOURCE	IDENTIFIER
Antibodies		
SARS-CoV-2 (2019-nCoV) Nucleocapsid Antibody, Rabbit MAb	Sino Biological	Cat#40588-R001
HRP-conjugated donkey anti rabbit IgG(H + L)	Jackson ImmunoResearch	Cat#711-035-152; RRID:AB_10015282
Ab[numbers]	This study	N/A
BV421 anti-human CD19 Antibody	BioLegend	Cat#302234; RRID:AB_11142678
PE anti-human IgD Antibody	BioLegend	Cat#348204; RRID:AB_10553900
APC/Cy7 anti-human CD27 Antibody	BioLegend	Cat#302816; RRID:AB_571977
PE/Cy7 anti-human CD20 Antibody	BioLegend	Cat#302312; RRID:AB_314260
InVivoMAb human IgG1 Iso-type control	Bio X cell	Cat#BE0297; RRID:AB_2687817
Imdevimab	Hansen et al.[16]	N/A
Bacterial and virus strains		
SARS-CoV-2 JPN/TY/WK-521	National Institute of Infectious Diseases	EPI_ISL_408667
SARS-CoV-2/UT-NCGM02/Human/2020/Tokyo	Imai et al.[22]	EPI_ISL_418809
SARS-CoV-2 Alpha variant (QHN002)	National Institute of Infectious Diseases	EPI_ISL_804008
SARS-CoV-2 Beta variant (TY8-612)	National Institute of Infectious Diseases	EPI_ISL_1123289
SARS-CoV-2 Gamma variant (TY7-503)	National Institute of Infectious Diseases	EPI_ISL_877769
SARS-CoV-2 Kappa variant (TY11-330)	National Institute of Infectious Diseases	EPI_ISL_2158613
SARS-CoV-2 Delta variant (TY11-927)	National Institute of Infectious Diseases	EPI_ISL_2158617
SARS-CoV-2 Omicron variant (BA.1, TY38-873)	National Institute of Infectious Diseases	EPI_ISL_7418017
SARS-CoV-2 Omicron variant (BA.2, TY40-158)	National Institute of Infectious Diseases	EPI_ISL_9595858
Escherichia coli strain DH5alpha	TOYOBO	Cat#DNA-903F
Chemicals, peptides, and recombinant proteins		
RBD-SBP	This paper	N/A
ACE2-SBP	This paper	N/A
ACE2-Flag	This paper	N/A
Polyethylenimine Max	Polyscience	Cat#24765-100
APC-conjugated streptavidin	eBioscience	Cat#17-4317-82
Anti-Aggregate Wash	Cellular Technology Limited	Cat#CTL-AA-010
Buffer RLT	QIAGEN	Cat#79216
2-mercaptoethanol	Thermo Fisher Scientific	Cat#21985023
RNAClean XP	Beckman Coulter	Cat#A63987
dNTP Mix	New England Biolabs	Cat#N0447L
KAPA HiFi HS ReadyMix	KAPA Biosystems	Cat#KK2602
EnduRen	Promega	Cat#E6481
20% formalin	Fujifilm Wako	Cat#064-03865
Cristal violet solution	Merck	Cat#V5265
Opti-MEM I	Thermo Fisher Scientific	Cat#31985070
Blocking One	NACALAI TESQUE	Cat#03953-95
Critical commercial assays		
FACS AriaIII	BD Biosciences	N/A
FACS Verse	BD Biosciences	N/A

(*Continued on next page*)

Continued

REAGENT or RESOURCE	SOURCE	IDENTIFIER
Octet K2	Forte Bio	Cat#Octet K2
Bright-GloTM Luciferase Assay system	Promega	Cat#E2610
GloMax Discover microplate reader	Promega	Cat#GM3000
Epoch 2	Agilent BioTek	Cat#EPOCH2NS
GenElute HP Plasmid Maxiprep Kit	Merck	Cat#NA0300
Expi293 Expression System	Thermo Fisher Scientific	Cat#A14635
BIACORE T200	Cytiva	N/A
Series S Sensor Chip CM5	Cytiva	BR100530
Vitrobot Mark IV system	Thermo Fisher Scientific	N/A
300 kV Titan Krios G4 transmission electron microscope	Thermo Fisher Scientific	N/A
BioQuantum K3 direct electron detector	Gatan	N/A
Quantifoil 0.6/1 Cu 300 mesh	E M Japan	Cat#M2947C-1
rapifleX MALDI Tissuetyper	Bruker Corporation	N/A
StepOnePlus	Thermo Fisher Scientific	Cat#4376598
CFX-96	BIO-RAD	Cat#1854095J1
405 TS washer	Agilent	N/A
Multi-Beads Shocker	YASUI KIKAI	Cat#MB3000
TaqMan Fast Virus 1-step Master Mix	Thermo Fisher Scientific	Cat#4444432
RNeasy Plus Mini Kit	QIAGEN	Cat#74136
HisTrap HP column	Cytiva	Cat#29051021
Superose 6 Increase10/300 GL column	Cytiva	Cat#29091596
Superdex200 10/300 GL column	Cytiva	Cat#28990944
Protein G Sepharose 4 Fast Flow resin	Cytiva	Cat#17061801
HisTrap HP column	Cytiva	Cat#17524801
Streptavidin Biosensors	Sartorius	Cat#18-5019
Anti-human IgG Fc Capture Biosensors	Sartorius	Cat#18-5060
Anti-DYKDDDDK tag Antibody Beads	Fujifilm Wako	Cat#018-22783
Streptavidin Sepharose High Performance	Cytiva	Cat#17511201
NEBuilder HiFi DNA Assembly Master Mix	New England BioLabs	E2621X
Ab Capcher Mag2	Protenova	Cat#P-052-10
Human IgG ELISA Quantitation Set	Bethyl Laboratories	Cat#E80-104
CD19 microbeads	Miltenyi Biotec	Cat#130-050-301
Deposited data		
Structure of Ab159 in complex with SARS-CoV-2-RBD	This paper	EMD: 33060 PDB: 7X8Y
Structure of Ab188 in complex with SARS-CoV-2-RBD	This paper	EMD: 33061 PDB: 7X8Z
Structure of Ab326 in complex with SARS-CoV-2-RBD	This paper	EMD: 33062 PDB: 7X90
Structure of Ab354 in complex with SARS-CoV-2-RBD	This paper	EMD: 33059 PDB: 7X8W
Structure of Ab445 in complex with SARS-CoV-2-RBD	This paper	EMD: 33064 PDB: 7X92

(*Continued on next page*)

Continued

REAGENT or RESOURCE	SOURCE	IDENTIFIER
Structure of Ab496(Fv-clasp) in complex with SARS-CoV-2-RBD	This paper	EMD: 33063 PDB: 7X91
Experimental models: Cell lines		
293T	RIKEN BRC	Cat#RCB2202
Expi293F	Thermo Fisher Scientific	Cat#R79007
293FT cell expressing SARS-CoV-2 Spike and DSP8-11	Yamamoto et al.[42]	N/A
293FT cell expressing hACE2, hTMPRSS2 and DSP1-7	Yamamoto et al.[42]	N/A
VeroE6/TMRRSS2 cell	JCRB Cell Bank	Cat#JCRB1819
Raji cells	JCRB Cell Bank	Cat#JCRB9012
Oligonucleotides		
SARS-CoV-1-Spike gene optimized	Eurofins Genomics	N/A
Omicron (BA.1)-Spike gene optimized	Eurofins Genomics	N/A
oligo-dT primer (5′-Biotin–AAGCAGT GGTATCAACGCAGAGTACT30VN-3′)	Hokkaido System Science	N/A
2019-nCoV_N1-F primer	Eurofins Genomics	Cat#CDC-01
2019-nCoV_N1-R primer	Eurofins Genomics	Cat#CDC-02
2019-nCoV_N1-P probe	Eurofins Genomics	Cat#CDC-03
Recombinant DNA		
pcDNA3.4 TOPO	Thermo Fisher Scientific	Cat#A14697
pcDNA3.4-Spike	Takeshita et al.[37]	N/A
pcDNA3.4-Spike series	This paper	N/A
pcDNA3.4-ACE2(1-708AA)-SBP	This paper	N/A
pcDNA3.4-ACE2(1-708AA)-Flag	This paper	N/A
pcDNA3.4-Spike(1-1213AA)-SBP	This paper	N/A
pcDNA3.4-S1(1-685AA)-SBP	This paper	N/A
pcDNA3.4-RBD(319-541AA)-SBP	This paper	N/A
pMX-GFP	CELL BIOLABS INC	Cat#RTV-050
pNL4-3.luc.R-E−	NIH	N/A
pCMV3_SARS-cov2d19 series	This paper	N/A
pcDNA3.4-Hexapro	This paper	N/A
pCR2.1- Ab496 Fv-clasp	This paper	N/A
pcDNA3.4-Ab[numbers]-H/L chain	This paper	N/A
Software and algorithms		
Octet Data Analysis Software	Sartorius	Version 10.0
FACSuite	BD Biosciences	Version 1.0.6
FACSDiva	BD Biosciences	Version 6.1.3
FlowJo	BD Biosciences	Version 15.0
GraphPad Prism	GraphPad Software	Version 9.3.1
EPU software	Thermo Fisher Scientific	Cat#1025707-J
RELION-3.1.2 package	Zivanov et al.[48]	N/A
MotionCor2	Zheng et al.[50]	N/A
CTFFIND4	Rohou and Grigorieff[51]	N/A
crYOLO	Wagner et al.[52]	N/A

(*Continued on next page*)

Continued

REAGENT or RESOURCE	SOURCE	IDENTIFIER
Phenix package	Liebschner et al.[53]	N/A
Coot	Emsley et al.[54]	N/A
SWISS-MODEL server	Waterhouse et al.[55]	N/A
MolProbity	Williams et al.[56]	N/A
PyMOL	https://pymol.org/2/	N/A
UCSF ChimeraX	Goddard et al.[57]	N/A
Mascot	Matrix Science Ltd	Version 2.7
GlyConnect database	Mariethoz et al.[59]	N/A
JMP	SAS Institute	Version 15.0.0

RESOURCE AVAILABILITY

Lead contact

Requests for resources and reagents should be directed to the Lead Contact Author Masaru Takeshita (takeshita@a5.keio.jp).

Materials availability

All unique reagents generated in this study are available from the lead contact with a completed Material Transfer Agreements.

Data and code availability

The cryo-EM maps and atomic models have been deposited at the Electron Microscopy DataBank and the PDB with the accession codes listed in Table S3, and are publicly available as of the date of publication. Additional data needed to support the conclusion of this manuscript are included in the main text and supplementary materials. This paper does not report original code. Any additional information required to reanalyze the data reported in this paper is available from the lead contact upon request.

EXPERIMENTAL MODEL AND SUBJECT DETAILS

Ethics statements

We recruited 47 patients who had COVID-19, diagnosed by approved reverse transcriptase polymerase chain reaction (RT-PCR) tests for SARS-CoV-2 using swabs from the nose or saliva, and hospitalized at Keio University Hospital between April and December 2020. Peripheral blood samples from patients were collected at outpatient visits after discharge. The following parameters were collected from medical charts: signs and symptoms; lymphocyte counts; serum parameters of lactate dehydrogenase (LD), C-reactive protein (CRP); and medication history. Disease severity is based on "COVID-19 Clinical Management," edited by the World Health Organization (25 Jan 2021). The patients' characteristics are shown in Table S1. This study was approved by the Ethics Committee of Keio University School of Medicine and conducted in compliance with the tenets of the Declaration of Helsinki. Informed consent was obtained from all participating individuals.

Animal studies

All experiments with hamsters were performed in accordance with the Science Council of Japan's Guidelines for Proper Conduct of Animal Experiments. The protocols were approved by the Animal Experiment Committee of the Institute of Medical Science, the University of Tokyo. The study included one-month-old male hamsters.

All experiments with macaques were performed in accordance with the Guidelines for the Husbandry and Management of Laboratory Animals of the Research Center for Animal Life Science at Shiga University of Medical Science and Standards Relating to the Care and Fundamental Guidelines for Proper Conduct of Animal Experiments and Related Activities in Academic Research Institutions under the jurisdiction of the Ministry of Education, Culture, Sports, Science and Technology, Japan. The protocols were approved

by the Shiga University of Medical Science Animal Experiment Committee. The study included eight-to nine-year-old female macaques.

Cells

293T and 293FT cells were maintained in DMEM containing 10% FCS and antibiotics at 37°C with 5% CO_2. Expi293F cells were maintained in Expi293 Expression Medium at 37°C with 8% CO_2. Vero E6/TMPRSS2 cells were maintained in low glucose DMEM containing 10% fetal bovine serum, antibiotics, and 1 mg/mL geneticin at 37°C with 5% CO_2. Raji cells were maintained in RPMI1640 containing 10% FCS.

METHOD DETAILS

Production of vectors and proteins

The extracellular domain of ACE2 (1–708 AA) was cloned into the pcDNA3.4 expression vector with a FLAG tag or a streptavidin-binding peptide (SBP) tag at the C-terminus. Double-stranded DNAs coding full-length Spike of SARS-CoV-2 (UniProtKB-P0DTC2) and SARS-CoV-1 (UniProtKB-P59594) were codon-optimized and synthesized and inserted into the pcDNA3.4 vector. The extracellular domain (1-1213AA), S1 (1-685AA), and RBD (319-541AA) was cloned into the pcDNA3.4 vector with an SBP tag at the C-terminus. The expression vectors of mutated Spike were prepared by PCR using mutated primers. Recombinant RBD and ACE2 were produced using the Expi293 Expression System, and purified using Anti-DYKDDDDK tag Antibody Beads and Streptavidin Sepharose High Performance beads.[37]

Cell-based Spike-ACE2 inhibition assay

The expression vector of full-length Spike or mutated Spike and pMX-GFP were cotransfected into 293T cells using Polyethylenimine Max. After 2 days, cells were washed with PBS supplemented with 0.5% BSA and 2 mM EDTA (staining buffer), incubated with diluted serum samples or antibodies, washed again, and incubated with premixed ACE2-SBP and APC-conjugated streptavidin. After the final wash, the cells were analyzed by a FACS Verse. The median fluorescent intensity (MFI) among GFP^+ cells was calculated using FlowJo and used as an indicator of Spike-ACE2 inhibition. The MFI of cells without serum or antibody were defined as 100% control and the ACE2-binding rate of serum or antibody was calculated as follows: ACE2-binding rate = 100 × (MFI of serum or antibody)/(MFI of control).[37] Some serum results measured in a previous paper[37] were used.

Cell sorting

Peripheral blood mononuclear cells (PBMCs) were stored at −80°C and thawed at 37°C using Anti-Aggregate Wash, incubated for 30 min with RPMI medium.[38] $CD19^+$ B cells were isolated by positive selection using CD19 Microbeads and stained with fluorochrome-conjugated antibodies and antigens for 20 min at 4°C. Plasma cells and antigen-specific memory B cells were defined as $CD19^+$ surface IgD^- $CD27^+$ $CD20^-$ $CD38^+$ and $CD19^+$ surface IgD^- $CD27^+$ $CD20^+$ $CD38^-$ Wuhan-RBD^+ Wuhan-$S1^+$, respectively, and sorted using a FACS Aria III flow cytometer.

Production of antibodies

The production of single-cell cDNA was performed using Smart-seq2[39] with some modifications. Briefly, cells were sorted into 5 μL of Buffer RLT with 1% 2-mercaptoethanol in a 96-well PCR plate. RNAs were bound to 11 μL of RNAClean XP, washed using 80% ethanol as per the manufacturer's instructions, and eluted by Elution buffer (2.3 μL of nuclease-free water, 1 μL of dNTP Mix, and 1 μL of modified oligo-dT primer. Subsequent reverse transcription PCR (23 cycles) and purification were performed as in Smart-seq2.[39]

The production of expression vectors was performed as previously described with some modifications.[40,41] First, PCR was performed with a total volume of 20 μL containing 1 μL of cDNA library, 300 nM of primer set1, and 10 μL of KAPA HiFi HS ReadyMix. The cycling parameters were as follows: 95°C for 3 min; 30 cycles at 98°C for 20 s, 65°C for 15 s, and 72°C for 30 s; and 72°C for 1 min. For IgG, subsequently, second PCR was performed using primer set2 in a total volume of 20 μL containing 1 μL of first PCR product, 300 nM of each primer, and 10 μL of KAPA HiFi HS ReadyMix with cycling parameters as follows: 95°C for 3 min; 30 cycles at 98°C for 20 s, 63°C for 15 s, and 72°C for 30 s; and 72°C for 1 min. The IgG, Igκ, and Igλ products of second PCR were electrophoresed, purified, and inserted into the expression vector for IgH or Igκ or Igλ using NEBuilder HiFi DNA Assembly Master Mix. When the second PCR failed to generate the appropriate

band, third PCR was performed using primer set3 in a total volume of 10 μL containing 0.5 μL of first PCR product, 300 nM of each primer, and 5 μL of KAPA HiFi HS ReadyMix with cycling parameters as second PCR. Third PCR products and second PCR products of IgA and IgM were sequenced. Fourth PCR was performed using primer set4 as in the second PCR, and the products were inserted into the expression vector. The primer list is shown in Table S4. For *in vivo* studies, variable regions were inserted into the expression vector that had N297A mutation introduced in the Fc region.

Monoclonal antibodies were produced by transient cotransfection of IgH and IgL vectors using the Expi293 Expression System for 5 or 6 days, purified using Ab Capcher Mag2, and quantified using Human IgG ELISA Quantitation Set.

Anti-Spike protein antibodies for animal study were expressed using the Expi293 Expression System according to the manufacturer's instructions. Culture media were harvested on day 7. The antibodies secreted were purified by Protein G Sepharose 4 Fast Flow resin, followed by gel filtration chromatography on a Superdex200 10/300 GL column equilibrated in PBS.

The sequences of variable region of selected antibodies were shown in Table S5.

Biolayer interferometry

The epitope binning assays were performed by biolayer interferometry using Octet K2 and its software. Streptavidin Biosensors were loaded by the extracellular domain of Spike (10 μg/mL) until the change in response reached 0.7 to 0.8 nm. After washing in kinetics buffer, the sensors were saturated with the first antibody (60 μg/mL) for 600 s. After confirming that the sensors were saturated by reacting 20 μg/mL of the first antibody, the sensors were reacted to 20 ug/ml of the second antibody to examine whether the two antibodies could bind simultaneously.

Fusion inhibition assay

The assay was modified from the dual split protein (DSP) assay.[42] Two 293FT cell lines, one expressing SARS-CoV-2 Spike protein and DSP8-11, and the other expressing human ACE2, human TMPRSS2, and DSP1-7, were used in this assay. Both cells were treated with the final 6 μM EnduRen in the concentration of 2×10^5/500 μL/well using 12-well plates. After making a single-cell suspension by pipetting, 50 μL (2×10^4 cells) of the Spike-expressing cell suspension was incubated with 10 μL of 10 μg/mL of antibody for 30 min at 37°C. Next, 50 μL (2×10^4 cells) of the human ACE2/TMPRSS2 protein-expressing cell suspension was added to the antibody–cell mix and incubated for 2.5 h at 37°C. The Renilla luciferase activity was measured using the GloMax Discover System.

Endpoint micro neutralization assay

Serially diluted sera were mixed with 100 TCID50 SARS-CoV-2 JPN/TY/WK-521 strain[43] and incubated at 37°C for 1 h. The mixtures were placed on VeroE6/TMRRSS2 cells. After 5 days, plates were fixed with 20% formalin and stained with crystal violet solution. The highest sera dilution factor with 100% CPE inhibition was defined as the micro neutralization titer.[43]

Pseudovirus neutralization assay

Two plasmids, pNL4-3.luc.R-E− and pCMV3_SARS-cov2d19 series generated from the codon optimized pCMV3_Spike (1-1254AA) were transfected into cells and the pseudovirus was produced using the Expi293 expression system. Twenty thousand cells/100 μL/well human ACE2/TMPRSS2-expressing 293FT cell line (DSP1-7[42] were seeded in a 96-well plate 1 day before infection. Serially diluted antibodies and 10,000 U/well viruses were mixed in 50 μL/well with DMEM containing 10% FCS, 1× MEM non-essential amino acids solution, and 1 mM sodium pyrubate, incubated for 37°C for 1 h. Fifty microliters per well of the cell culture supernatant were removed and the antibody–virus mixture was applied to the cell layer. After 48 h, the supernatant was removed completely and 50 μL/well of the Glo lysis buffer was added. After 5 min agitation, the plate was frozen at −80°C. After being thawed and agitated, 10 μL of the lysate was subjected to the Bright-GloTM Luciferase Assay system using a GloMax Discover microplate reader. The data from biological triplicates was analyzed using Prism 9 to determine the value of IC_{50} (ng/mL).

Authentic virus neutralization assay

For Wuhan strain and Alpha, Beta, Gamma, and Kappa variant, eighteen thousand cells/well VeroE6/TMPRESS2 were seeded in a 96-well plate 1 day before infection. After the cell layers was washed with PBS, serially diluted antibodies and 100TCID50/well viruses were mixed in DMEM low glucose containing 2% FCS incubated for 37°C for 1 h, and applied to the cell layers. After 20 to 24 h, the cells were fixed, dried, and subjected to enzyme-linked immunosorbent assay (ELISA). The cells were washed with PBS containing 0.3% Tween 20 (v/v) as washing buffer three times and stained with rabbit anti-SARS-COV-2 nucleocapsid monoclonal antibodies in 5% Blocking One–containing washing buffer. After washing three times, the cells were incubated with HRP-conjugated donkey anti rabbit IgG(H + L) followed by washing and TMB colorimetric assay. Each sample was assayed in triplicate. All washing processes were performed using a 405 TS washer.

For Delta and Omicron (BA.1 and BA.2) variant, neutralization assays were performed as previously described[44] with minor modifications. Briefly, a mixture of 100 TCID50 virus and serially diluted antibodies was incubated at 37C for 1 h before being placed on VeroE6/TMPRSS2 cells seeded in 96-well flat-bottom plates. After culturing for 4–5 days at 37C supplied with 5% CO2, cells were fixed with 20% formalin and stained with crystal violet solution. Each sample was assayed in duplicate. Absorbance at 595 nm was measured using Epoch 2 area scanning mode and the neutralization percentage was calculated as follows; (sample signals – virus control signals)/(cell-only control signals – virus control signals) x 100. The data from biological triplicates were analyzed using Prism 9 to determine the value of IC_{50} (ng/mL).

Viral uptake mediated by Fc receptors

Pseudovirus (Wuhan-hu-1 strain) was incubated with serially diluted antibody (3-fold; starting from 20 μg/mL) for 1 h at 37°C. The mixture of the antibody and the pseudovirus was applied to Raji cells. After incubating for 3 days at 37°C, the washed cells were lysed, and 10 μL of lysate was subjected to the luciferase assay.

Production of proteins for cryo-EM

cDNA for the stabilized variant of SARS-CoV-2 Spike protein (residues 1–1208) with 6 beneficial proline substitutions (F817P/A892P/A899P/A942P/K986P/V987P) and "GSAS" substitution at the furin cleavage site (residues 682–685), named HexaPro,[45] was subcloned into the pcDNA3.4 vector using PCR and In-Fusion Reaction. The above mutated Spike protein was designed to form a closed trimer by fusion with the C-terminal foldon trimerization motif followed by the TEV protease cleavage site, AviTag and 6xHis tag. cDNAs for heavy and light chains of the anti-Spike protein antibodies and their Fab heavy chain (VH-CH1) attached with the C-terminally TEV protease cleavage site and 6xHis tag were respectively subcloned downstream of the Ig kappa signal peptide into the pcDNA3.4 vector. Plasmid DNA was prepared using a GenElute HP Plasmid Maxiprep Kit.

Each protein was expressed using the Expi293 Expression System according to the manufacturer's instructions. Culture media were harvested on day 4 for the Spike protein variant and day 7 for Fab. The Spike protein variant secreted in the culture medium was purified by a HisTrap HP column, followed by gel filtration chromatography on a Superose 6 Increase10/300 GL column equilibrated in 20 mM Tris-HCl (pH8.0) and 150 mM NaCl. The secreted Fabs were purified with a HisTrap column, followed by gel filtration chromatography on a Superdex200 10/300 GL column equilibrated in 20 mM Tris-HCl (pH8.0) and 150 mM NaCl.

Ab496 Fv-clasp was designed[46] and cloned into a pCR2.1 TOPO TA cloning vector with an N-terminal His-tag and a TEV cleavage site fused to the VH and VL, respectively. Fv-clasp for Ab496 was synthesized at 25°C for 5 h in the presence of 5 mM GSSG and 0.4 mg/mL DsbC with the dialysis mode of the *Escherichia coli* cell-free protein synthesis method optimized to form disulfide bonds.[47,48] After the cell-free protein synthesis, the reaction solution was applied on a HisTrap HP column and the target protein was eluted with a linear gradient of imidazole. The His-tag was then cleaved by TEV protease and was removed by a HisTrap HP column. The protein was further purified by gel filtration chromatography on a Superdex200 10/300 GL column in 20 mM Tris-HCl (pH8.0) and 150 mM NaCl.

Cryo-EM data acquisition

The purified spike proteins (0.7 mg/ml of the trimer) and each antibody were mixed with a molar ratio of 1:9, and incubated at 4°C for 30 min. The mixture (3 μL) was applied onto a freshly glow-discharged holey carbon grid, coated with a single or two layers of graphene oxide, then blotted for 3 s at 4°C in 100% humidity and plunge-frozen in liquid ethane using the Vitrobot Mark IV system.

Cryo-EM imaging of the complex was performed on a 300 kV Titan Krios G4 transmission electron microscope equipped with a BioQuantum K3 direct electron detector in the electron counting mode. The imaging was performed at a nominal magnification of ×105,000, corresponding to a calibrated pixel size of 0.829 Å/pixel. Each micrographic movie was recorded for a total of 15.5 electrons per pixel per second for 2.3 s, resulting in an accumulated exposure of 50.5 e−/A2. A total of ∼12,000 movies were collected per dataset. All of the data were automatically acquired using the EPU software, with a defocus range of −0.8 to −2.0 μm.

Image processing

Image processing was mainly performed with the RELION-3.1.2 package.[49] All of the dose-fractionated movies were subjected to beam-induced motion correction using MotionCor2,[50] and the contrast transfer function (CTF) parameters were estimated using CTFFIND4.[51] Particles were picked using crYOLO[52] from the micrographs and subjected to several rounds of 2D and 3D classifications to select good particles, and subsequently subjected to 3D refinement and Bayesian polishing. In the last cycle, particles were refined with a specific mask (imposing C3 symmetry on some complexes), yielding an overall map with a global resolution of 3.6 to 2.4 Å. To further improve the density of Fab moieties, the particles were subjected to focused 3D classification using a soft mask encompassing the RBD and variable domains of Fabs. The best-resolved and locally refined density maps were sharpened by the Phenix package.[53] Reported resolutions are based on the Fourier shell correlation of 0.143 criterion.

Model building and validation

The trimeric structures of the spike protein with each Fab were manually fitted and constructed based on a structure (PDB ID: 6VXX) as an initial model, using Coot.[54] The template model of the variable domain was automatically built by the SWISS-MODEL server,[55] based on selected sequences with higher homology, and was manually fit in Coot.[54] In the spike moiety, several prominent densities were identified near Asparagine residues, which corresponded to N-glycosylation. Glucosamines (NAG) were built depending on each density size. The model of the entire structure was iteratively refined using phenix.real_space_refine of the Phenix package,[53] with secondary structure restrains. Model validation for stereochemistry was performed in MolProbity[56] (Table S3). Molecular graphics and density maps were prepared with PyMOL (https://pymol.org/2/) and UCSF ChimeraX.[57]

Identification of *N*-glycan composition

The Ab354 antibody sample purified from HEK cells contains one *N*-glycosylation site at the Asn59 of the heavy chain, and the SDS-PAGE analysis revealed its heterogeneous modification. As previously described,[58] ∼1 nmol of the sample was digested by trypsin, and then treated with PNGase F to remove *N*-linked glycans as a control. Signals of glycopeptide from the positive fraction were detected using matrix-associated laser desorption/ionization time-of-flight (MALDI-TOF) mass spectrometry. Four major peaks were detected and subjected to estimate the glycan components by using Mascot. The four peaks were attributed to + dHex(3)Hex(4)HexNAc(5), +dHex(2)Hex(4)HexNAc(5), +dHex(1)Hex(4)HexNAc(5), and dHex(1)Hex(3)HexNAc(5). (To confirm the relative difference of each glycan unit, each fraction was further applied to LC-MS/MS.) Referring to the GlyConnect database,[59] possible glycan forms were listed (Figure S2A). The traceable glycan model was reasonably placed near the Asn59 along the electron density, and fucose is identified, which is linked α-1,6 to the reducing terminal of β-*N*-acetylglucosamine, as shown in the Figures S2B and S2C.

Surface Plasmon Resonance (SPR) assay

SPR assay was performed using BIACORE T200 instrument. The SBP tagged RBD was covalently immobilized on CM5 sensor chip. Different concentrations of antibody solutions (0, 62.5, 125, 250, 500, 1000 ng/mL) were then sequentially pumped at a flow rate of 60 μL/mL and sensorgrams were obtained. The binding rate constant (kon), dissociation rate constant (koff), and dissociation constant (kd) for each sample were

obtained by curve fitting the sensorgrams with a 1:1 binding model. Data are representative of duplicate measurements.

Experimental infection of Syrian hamsters

SARS-CoV-2/UT-NCGM02/Human/2020/Tokyo[22] was propagated in VeroE6 cells in Opti-MEM I containing 0.3% BSA and 1 μg of L-1-Tosylamide-2-phenylethyl chloromethyl ketone (TPCK)-trypsin/mL. One-month-old male Syrian hamsters (Japan SLC Inc., Shizuoka, Japan) were used in this study. Four hamsters per group were inoculated intranasally with 10^3 PFU (in 100 μL) of NCGM02. On day 1 post-infection, hamsters were injected intraperitoneally with 50 mg/kg of Ab326, Ab354, Ab496, or human IgG1 Isotype control. The animals were euthanized on day 4 post-infection, and serum and lungs were harvested. Serum neutralizing titers were determined by using a plaque assay, and viral RNA copy numbers in the lung tissue were determined by RT-PCR.

For the neutralization assay, 35 μL of virus (140 tissue culture infectious dose 50) was incubated with 35 μL of 2-fold serial dilutions of serum for 1 h at room temperature, and 50 μL of the mixture was then added to confluent VeroE6/TMPRSS2 cells in 96-well plates, and incubated for 1 h at 37°C. After the addition of 50 μL of DMEM containing 5% FCS, the cells were incubated for 3 more days at 37°C. Viral cytopathic effects (CPEs) were observed under an inverted microscope and virus neutralization titers were determined as the reciprocal of the highest serum dilution that completely prevented CPEs.

For the RT-PCR, lung tissue was homogenized in 1 mL of DMEM containing 5% FCS and antibiotics. RNAs were extracted by using the QIAamp Viral RNA Mini Kit. RNA copies for the nucleoprotein (N protein)-encoding gene of SARS-CoV-2 were measured by using the TaqMan Fast Virus 1-step Master Mix. Amplification was carried out in 96-well plates on the StepOnePlus or CFX-96. The thermocycling conditions were as follows: 5 min at 50°C for reverse transcription, 20 s at 95°C for inactivation of reverse transcriptase and initial denaturation, and 45 cycles of 5 s at 95°C and 30 s at 60°C for amplification.

Experimental infection of cynomolgus macaques

We performed *in vivo* infection assay using cynomolgus macaques as previously described[23] with some modifications. Briefly, 2×10^7 $TCID_{50}$ WK-521 was inoculated into the conjunctiva, nasal cavity, oral cavity, and trachea of six cynomolgus macaques on day 0. On day 1, 20 mg (5–7 mg/kg) of antibody cocktail ($^1/_3$ each of Ab326, Ab354, and Ab496) or control human IgG1 was injected intravenously. Nasal swabs were collected at day 0 (before infection), day 1 (before injection), day 3, day 5, and day 7 (before sacrifice). Macaques were sacrificed at day 7, and lungs were collected.

To assess viral replication, serial dilutions of swab samples and tissue homogenate samples (10% w/v) were inoculated onto confluent VeroE6/TMPRSS2 cells for 1 h. The cells were washed with HBSS, and incubated with DMEM containing 0.1% BSA, penicillin, streptomycin, and gentamycin (50 μg/mL) for 3 days. CPEs were examined under a microscope. Virus titers were calculated by the Reed-Muench method.

To assess the viral amount at the nucleotide level, total RNA samples were extracted from swab samples using the QIAamp Viral RNA Mini Kit and RNeasy Plus Mini Kit according to the manufacturer's instructions. RNA copies were measured as described above.

To assess the neutralization titer, plasma collected on day 1 before antibody injection and on day 3 was incubated at 56°C for 1 h for complement inactivation. Diluted plasma was mixed with WK-521 for 30 min in room temperature. The mixture was inoculated onto confluent culture of VeroE6/TMPRSS2 cells in 6-well plates. After 1h, the mixture was removed and the cells were covered with EMEM containing 1% agar. The cells were incubated at 37°C for 3 days and the number of plaques was counted.

For histopathological examination, eight lung specimens were made from the bilateral lung of each macaque: one slice from each upper lobe and middle lobe, and two slices from each lower lobe. After fixing in 10% neutral buffered formalin for approximately 72 h, hematoxylin and eosin staining sections were made. Two pathologists blindly evaluated the histological score of the sections according to the previously published following criteria[24]: 0: normal lung, 1: mild destruction of bronchial epithelium, 2: mild peribronchiolar inflammation, 3: inflammation in the alveolar walls resulting in alveolar thickening, 4: mild alveolar injury accompanied by vascular injury, 5: moderate alveolar injury and vascular injury, 6, 7: severe alveolar

injury with hyaline membrane-associated alveolar hemorrhage (under or over 50% of the section area). The average score of eight sections was calculated for each macaque, and the mean score of the two pathologists was defined as the histological score.

QUANTIFICATION AND STATISTICAL ANALYSIS

Continuous data are presented as the median and interquartile range or as a number with the percentage value, as appropriate. Student's *t* test and Dunnett's test were used to examine the continuous variables. Chi-squared test was used to examine the categorical variables. Correlations between two continuous variables were analyzed using Spearman's rank correlation coefficient. Unless stated otherwise, statistical analyses were performed using JMP. IC_{50} of each antibody were determined by non-linear regression using Prism 9, and shown in mean and SD The sample sizes for the animal studies were determined from previous studies. The researchers were not blinded to the group allocations during the experiments. p values < 0.05 were considered to be statistically significant. $^{*}p < 0.05$.